



Article

Effectiveness of Natural Antioxidants against SARS-CoV-2? Insights from the *In-Silico* World

Muhammad Fayyaz ur Rehman ^{1,2,*}, Shahzaib Akhter ², Aima Iram Batool ³, Zeliha Selamoglu ⁴, Mustafa Sevindik ⁵, Rida Eman ², Muhammad Mustaqeem ⁶, Muhammad Safwan Akram ^{7,8}, Fariha Kanwal ⁹, Changrui Lu ^{1,*} and Mehwish Aslam ^{10,*}

- ¹ Department of Chemistry, Chemical Engineering and Biotechnology, Donghua University, Shanghai 201620, China
- ² Institute of Chemistry, University of Sargodha, Sargodha 41600, Pakistan; shahzaibakhter740@gmail.com (S.A.); ridaykhanuos@gmail.com (R.E.)
- ³ Department of Zoology, University of Sargodha, Sargodha 41600, Pakistan; aima.iram@uos.edu.pk
- ⁴ Department of Medical Biology, Faculty of Medicine, Nigde Omer Halisdemir University, Nigde 51240, Turkey; zselamoglu@ohu.edu.tr
- ⁵ Department of Food Processing, Bahçe Vocational School, Osmaniye Korkut Ata University, Osmaniye 80000, Turkey; sevindik27@gmail.com
- ⁶ Department of Chemistry, University of Sargodha, Bhakkar Campus, Bhakkar 30000, Pakistan; muhammad.mustaqeem@uos.edu.pk
- ⁷ School of Health and Life Sciences, Teesside University, Middlesbrough TS1 3BA, UK; safwan.Akram@tees.ac.uk
- ⁸ National Horizons Centre, Teesside University, Darlington DL1 1HG, UK
- ⁹ Med-X Research Institute, School of Biomedical Engineering, Shanghai Jiao Tong University, Shanghai 201620, China; farihakaanwal@gmail.com
- ¹⁰ School of Biological Sciences, University of the Punjab, Lahore 54600, Pakistan
- * Correspondence: muhammad.fayyaz@uos.edu.pk (M.F.u.R.); crlu@dh.u.edu.cn (C.L.); maslam.sbs@pu.edu.pk (M.A.)



Citation: Rehman, M.F.u.; Akhter, S.; Batool, A.I.; Selamoglu, Z.; Sevindik, M.; Eman, R.; Mustaqeem, M.; Akram, M.S.; Kanwal, F.; Lu, C.; et al.

Effectiveness of Natural Antioxidants against SARS-CoV-2? Insights from the *In-Silico* World. *Antibiotics* **2021**, *10*, 1011. <https://doi.org/10.3390/antibiotics10081011>

Academic Editors: Mohamed-Elamir F. Hegazy, Paul W. Pare and Ahmed Atef El-Beih

Received: 1 August 2021

Accepted: 16 August 2021

Published: 20 August 2021

Publisher's Note: MDPI stays neutral with regard to jurisdictional claims in published maps and institutional affiliations.



Copyright: © 2021 by the authors. Licensee MDPI, Basel, Switzerland. This article is an open access article distributed under the terms and conditions of the Creative Commons Attribution (CC BY) license (<https://creativecommons.org/licenses/by/4.0/>).

Abstract: The SARS CoV-2 pandemic has affected millions of people around the globe. Despite many efforts to find some effective medicines against SARS CoV-2, no established therapeutics are available yet. The use of phytochemicals as antiviral agents provides hope against the proliferation of SARS-CoV-2. Several natural compounds were analyzed by virtual screening against six SARS CoV-2 protein targets using molecular docking simulations in the present study. More than a hundred plant-derived secondary metabolites have been docked, including alkaloids, flavonoids, coumarins, and steroids. SARS CoV-2 protein targets include Main protease (M^{Pro}), Papain-like protease (PL^{Pro}), RNA-dependent RNA polymerase (RdRp), Spike glycoprotein (S), Helicase (Nsp13), and E-Channel protein. Phytochemicals were evaluated by molecular docking, and MD simulations were performed using the YASARA structure using a modified genetic algorithm and AMBER03 force field. Binding energies and dissociation constants allowed the identification of potentially active compounds. Ligand-protein interactions provide an insight into the mechanism and potential of identified compounds. Glycyrrhizin and its metabolite 18-β-glycyrrhetic acid have shown a strong binding affinity for M^{Pro}, helicase, RdRp, spike, and E-channel proteins, while a flavonoid Baicalin also strongly binds against PL^{Pro} and RdRp. The use of identified phytochemicals may help to speed up the drug development and provide natural protection against SARS-CoV-2.

Keywords: SARS CoV-2; Glycyrrhizin; Baicalin; Hesperidin; natural antivirals; antioxidants for COVID-19; inverse docking; human blood proteins

1. Introduction

SARS-CoV-2 (Severe Acute Respiratory Syndrome Coronavirus 2) originated in the Wuhan province of Central China in December 2019 [1] and its disease, COVID-19, was declared as a pandemic on 11 March 2020, after the infection spread globally [2]. This

disease has affected more than 204 million people and claimed more than 4.31 million lives around the globe [3]. Thanks to vaccines, the recovery rate from COVID-19 is getting better from 70 to 90%, but the battle between the virus and humans is continued. Unfortunately, despite all efforts and worldwide scientific contributions, no specific medicines are available. The SARS-CoV-2 variants have worsened the situation, especially in countries like India, USA, and Brazil, where COVID-19 infections have crossed 77 million [3]. The rise of the SARS-CoV-2 delta variant requires better disease management as vaccinated people, including adults and children, seem to be susceptible to infection. Though the mass vaccination in the last months has decreased the severity of the disease [4], there is still a need for effective and broadly accessible remedies. Global vaccination and the emergence of a COVID-19 free world may take years, especially in the least developed countries. Moreover, new SARS-CoV-2 variants may affect the vaccination process by reducing the efficacy and efficiency of the developed vaccines. Furthermore, neutralizing/spike antibodies responses from vaccines are not sufficient to protect the people with health complications/comorbidities from COVID-19 [5]. Herbal medicines and natural therapeutics consisting of phytochemical extracts provide safe interventions to treat various viral infections using novel mechanisms. Secondary metabolites from plants and mushrooms have shown different biological effects including antioxidants, antimicrobials, and anti-cancer activities [6–8]. Natural antivirals with the least toxicity are the best choice against coronaviruses [2,9–11]. Many of these phytochemicals not only provide antiviral activity but also act as antioxidants to tame interleukin storm and ROS damage during COVID-19.

SARS-CoV-2 is a beta coronavirus that uses its glycosylated surface spike (S) protein to interact with the angiotensin-converting enzyme II (ACE2) receptors present in the host cells. SARS-CoV-2 attacks the lower respiratory tract to cause viral pneumonia. It can infect the gastrointestinal tract, heart, kidney, liver, and central nervous system, leading to multiple organ failure [2]. The common symptoms of virus infection include high fever, dry cough, muscle pain, fatigue, diarrhea, and shortness of breath, while the complications of COVID-19 include Acute respiratory distress syndrome (ARDS), sepsis, kidney failure, and cardiac injury [12–14]. The federal drug authority (FDA) takes an average of 12 years to approve a drug or vaccine for any disease [15]. Therefore, a number of antivirals, antibiotics, and other FDA-approved drugs have been repurposed to treat COVID-19 [16]. A combination of an anti-arthritis drug, Hydroxychloroquine, and an antibiotic, azithromycin, was reported as a treatment of choice for COVID-19 due to their additional antiviral properties against many viruses, including Ebola, HIV, and SARS [17–24].

Later, the same drugs were found to increase the mortality rate in the COVID-19 patients [25,26] by causing arrhythmia and heart failure [27,28]. Monoclonal antibodies like Tocilizumab and Sarilumab [29–31], convalescent blood plasma [32,33], Camostat mesylate [34], β -interferon [35], Corticosteroids [36] have also been used against COVID-19 patients, but these treatments are costly as well as coming with long term side effects. Recently, a non-FDA-approved antiviral drug, Remdesivir, has been allowed for emergency use against COVID-19, but the drug is costly and still requires large non-randomized trials for safe use [37]. Most of these therapeutics target SAS-CoV-2 key proteins, including main protease (M^{Pro}), Papain-like protease (PL^{Pro}), RNA-dependent RNA polymerase (RdRNA polymerase), Spike glycoprotein (S), and helicase (Figure 1). In silico studies provide a quicker method to screen large libraries of those naturally existing in a few hours to days. In this study, we have screened more than a hundred natural compounds including Phenolics, Flavonoids, Saponins, Steroids, against six different proteins of SARS-CoV-2, with an aim to identify potential bioactivity, using molecular docking and molecular dynamic simulations (MDS).

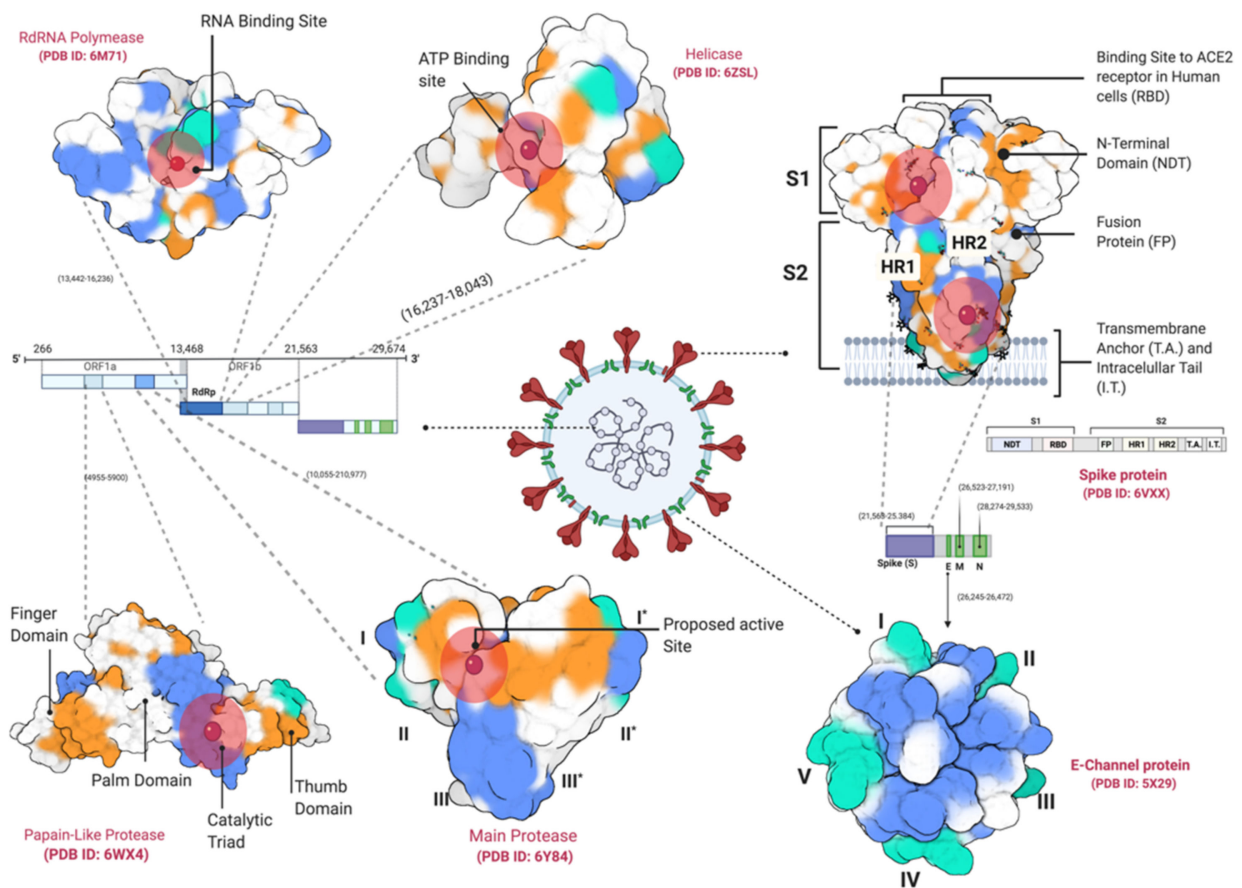


Figure 1. SARS-CoV-2 target proteins including Main Protease (M^{Pro} , * shows domains in the second subunit of the enzyme), Papain-like Protease (PL^{Pro}), RNA-dependent RNA polymerase (RdRNA polymerase), Spike glycoprotein (S), helicase, and E-Channel protein.

2. Results

2.1. Main Protease (M^{Pro})

The phytochemical ligands in this investigation were screened against M^{Pro} . The ligands with the best docking against the Main Protease are listed in Table 1. Glycyrrhizin, 18, β -Glycyrrhetic acid, Rhodiolin, Baicalin, and Silymarin were the best five ligands with high binding energies and dissociation constants (Figure 2). Glycyrrhizin showed binding to M^{Pro} at two different binding sites with the highest binding scores of -9.57 and -9.46 kcal·mol $^{-1}$ and a dissociation constant of 0.11 and 0.76 μ M. The best Glycyrrhizin binding site is the conventional M^{Pro} active site located between domains I and II. This site mainly consists of Thr 24 , Thr 25 , Thr 26 , Leu 27 , His 41 , Cys 45 , Ser 46 , Met 49 , Tyr 18 , Asn 119 , Asn 142 , Gly 143 , Cys 145 , His 163 , His 164 , Met 165 , Gly 166 , and Gln 189 , where Thr 26 and Gly 143 formed H-bonds with the Glycyrrhizin (Figure 2, Table 1). His 41 and Cys 145 are the key residues involved in the enzyme active site and have been previously defined in M^{Pro} active site by an X-ray crystallographic structure (PDB ID 6WQF) obtained at room temperature [38]. The His 41 and Cys 145 form a catalytic dyad that interacts with the bound ligand. Other amino acids in the proposed active site Ser 46 , Leu 141 , Asn 142 , Glu 166 , Pro 168 , Gln 189 , Thr 190 , and Ala 191 [38,39] were found involved in the stabilization of the enzyme active site.

Table 1. The best five docked ligands to Main Protease, Papain-like protease, RNA-dependent RNA polymerase, Spike Glycoprotein and Helicase, E-Channel; their binding energies, dissociations constants and active site residues.

Target	Phytochemicals	Binding Energy (kcal/mol)	Dissociation Constant (μ M)	Active Site Residue
Main Protease (M^{Pro})	Glycyrrhizin	−9.57	0.11	Thr ²⁴ , Thr ²⁵ , Thr ²⁶ , Leu ²⁷ , Gly ²⁹ , His ⁴¹ , Cys ⁴⁴ , Ser ⁴⁶ , Met ⁴⁹ , Tyr ¹¹⁸ , Asn ¹¹⁹ , Asn ¹⁴² , Gly ¹⁴³ , Cys ¹⁴⁵ , His ¹⁶³ , His ¹⁶⁴ , Met ¹⁶⁵ , Glu ¹⁶⁶
		−9.46	0.76	Arg ¹³¹ , Asn ¹³³ , Thr ¹³⁵ , Val ¹³⁷ , Thr ¹⁶⁹ , Val ¹⁷¹ , Ala ¹⁹⁴ , Gly ¹⁹⁵ , Thr ¹⁹⁶ , Asp ¹⁹⁷ , Thr ¹⁹⁸ , Thr ¹⁹⁹ , Tyr ²³⁷ , Asn ²³⁸ , Tyr ²³⁹ , Leu ²⁷² , Leu ²⁸⁶ , Leu ²⁸⁷ , Asp ²⁸⁹
	18,β-Glycyrrhetic acid	−9.19	0.35	Lys ⁵ , Arg ¹³¹ , Lys ¹³⁷ , Asp ¹⁹⁷ , Thr ¹⁹⁹ , Tyr ²³⁷ , Tyr ²³⁹ , Leu ²⁷² , Leu ²⁸⁶ , Leu ²⁸⁷ , Glu ²⁸⁸ , Asp ²⁸⁹ , Glu ²⁹⁰
	Rhodiolin	−9.05	0.23	Thr ²⁵ , His ⁴¹ , Cys ⁴⁴ , Thr ⁴⁵ , Ser ⁴⁶ , Met ⁴⁹ , Leu ¹⁴¹ , Asn ¹⁴² , Gly ¹⁴³ , Ser ¹⁴⁴ , Cys ¹⁴⁵ , His ¹⁶³ , Met ¹⁶⁵ , Glu ¹⁶⁶ , Leu ¹⁶⁷ , Pro ¹⁶⁸ , Arg ¹⁸⁸ , Gln ¹⁸⁹ , Thr ¹⁹⁰ , Gln ¹⁹²
	Baicalin	−8.85	0.33	Val ¹⁰⁴ , Ile ¹⁰⁶ , Gln ¹¹⁰ , Thr ¹¹¹ , Asn ¹⁵¹ , Ile ¹⁵² , Asp ¹⁵³ , Tyr ¹⁵⁴ , Pro ²⁵² , Thr ²⁹² , Phe ²⁹⁴ , Asp ²⁹⁵ , Val ²⁹⁷ , Arg ²⁹⁸ , Val ³⁰³
Papain like protease (PL^{Pro})	Silymarin	−8.71	0.41	Thr ²⁴ , Thr ²⁵ , Thr ²⁶ , Leu ²⁷ , His ⁴¹ , Cys ⁴⁴ , Thr ⁴⁵ , Ser ⁴⁶ , Met ⁴⁹ , Gly ¹⁴³ , Cys ¹⁴⁵ , His ¹⁶⁴ , Met ¹⁶⁵ , Glu ¹⁶⁶ , Leu ¹⁶⁷ , Pro ¹⁶⁸ , Arg ¹⁸⁸ , Gln ¹⁸⁹ , Thr ¹⁹⁰ , Gln ¹⁹²
	Baicalin	−10.82	0.01	Cys ¹⁵⁵ , Asn ¹⁵⁶ , Lys ¹⁵⁷ , Glu ¹⁶¹ , Leu ¹⁶² , Gly ¹⁶³ , Asp ¹⁶⁴ , Val ¹⁶⁵ , Arg ¹⁶⁶ , Glu ¹⁶⁷ , Tyr ¹⁷¹ , Val ²⁰² , Met ²⁰⁶ , Met ²⁰⁸ , Pro ²⁴⁸ , Tyr ²⁶⁴ , Tyr ²⁶⁸ , Gln ²⁶⁹ , Tyr ²⁷³
	Hesperidin	−10.61	0.02	Lys ¹⁵⁷ , Thr ¹⁵⁸ , Glu ¹⁶¹ , Leu ¹⁶² , Gly ¹⁶³ , Asp ¹⁶⁴ , Val ¹⁶⁵ , Glu ¹⁶⁷ , Leu ¹⁹⁹ , Glu ²⁰³ , Tyr ²⁰⁷ , Met ²⁰⁸ , Lys ²³² , Pro ²⁴⁸ , Tyr ²⁶⁴ , Tyr ²⁶⁸ , Gln ²⁶⁹ , Cys ²⁷⁰ , Tyr ²⁷³ , Thr ³⁰¹
	Naringen	−10.17	0.04	Cys ¹⁵⁵ , Asn ¹⁵⁶ , Glu ¹⁶¹ , Leu ¹⁶² , Gly ¹⁶³ , Asp ¹⁶⁴ , Arg ¹⁶⁶ , Gln ¹⁶⁷ , Ser ¹⁷⁰ , Leu ¹⁸⁵ , Leu ¹⁹⁹ , Val ²⁰² , Glu ²⁰³ , Met ²⁰⁶ , Tyr ²⁰⁷ , Met ²⁰⁸ , Ile ²²² , Pro ²²³ , Lys ²³² , Tyr ²⁶⁸
	Flemiflavanone D	−10.07	0.04	Lys ¹⁵⁷ , Glu ¹⁶¹ , Leu ¹⁶² , Gly ¹⁶³ , Asp ¹⁶⁴ , Arg ¹⁶⁶ , Glu ¹⁶⁷ , Ser ¹⁷⁰ , Val ²⁰² , Glu ²⁰³ , Met ²⁰⁶ , Tyr ²⁰⁷ , Met ²⁰⁸ , Tyr ²⁶⁴ , Tyr ²⁶⁸ , Gln ²⁶⁹ , Tyr ²⁷³
RNA-dependent RNA polymerase (RdRP)	Euchrestaflavanone A	−9.95	0.05	Lys ¹⁵⁷ , Glu ¹⁶¹ , Leu ¹⁶² , Gly ¹⁶³ , Asp ¹⁶⁴ , Arg ¹⁶⁶ , Glu ¹⁶⁷ , Ser ¹⁷⁰ , Val ²⁰² , Glu ²⁰³ , Met ²⁰⁶ , Tyr ²⁰⁷ , Met ²⁰⁸ , Tyr ²⁶⁸
	Glycyrrhizin	−10.52	0.03	Asp ⁴⁵² , Tyr ⁴⁵⁵ , Lys ⁵⁵¹ , Arg ⁵⁵³ , Ala ⁵⁵⁴ , Arg ⁵⁵⁵ , Thr ⁵⁵⁶ , Trp ⁶¹⁷ , Asp ⁶¹⁸ , Tyr ⁶¹⁹ , Pro ⁶²⁰ , Lys ⁶²¹ , Cys ⁶²² , Asp ⁶²³ , Arg ⁶²⁴ , Ser ⁷⁵⁹ , Asp ⁷⁶⁰ , Asp ⁷⁶¹ , Ala ⁷⁶² , Lys ⁷⁹⁸ , Cys ⁷⁹⁹ , Trp ⁸⁰⁰ , Glu ⁸¹¹ , Phe ⁸¹² , Cys ⁸¹³ , Ser ⁸¹⁴
		−9.96	0.05	Asp ⁴⁵² , Tyr ⁴⁵⁵ , Arg ⁵⁵³ , Ala ⁵⁵⁴ , Arg ⁵⁵⁵ , Trp ⁶¹⁷ , Asp ⁶¹⁸ , Lys ⁶²¹ , Cys ⁶²² , Asp ⁶²³ , Arg ⁶²⁴ , Ser ⁷⁵⁹ , Asp ⁷⁶⁰ , Asp ⁷⁶¹ , Lys ⁷⁹⁸ , Trp ⁸⁰⁰ , Glu ⁸¹¹ , Cys ⁸¹³ , Ser ⁸¹⁴
	Hesperidin	−9.53	0.1	Val ¹⁶⁶ , Tyr ⁴⁵⁶ , Met ⁵⁴² , Arg ⁵⁵³ , Ala ⁵⁵⁴ , Arg ⁵⁵⁵ , Thr ⁵⁵⁶ , Val ⁵⁵⁷ , Ala ⁵⁵⁸ , Asp ⁶¹⁸ , Tyr ⁶¹⁹ , Pro ⁶²⁰ , Lys ⁶²¹ , Cys ⁶²² , Asp ⁶²³ , Arg ⁶²⁴ , Lys ⁶⁷⁶ , Thr ⁶⁸⁰ , Ser ⁶⁸¹ , Ser ⁶⁸² , Phe ⁷⁹³ , Ser ⁷⁹⁵ , Lys ⁷⁹⁸
	Baicalin	−9.01	0.25	Val ³¹ , Tyr ³² , Lys ⁴⁷ , Tyr ¹²⁹ , Ala ¹³⁰ , His ¹³³ , Phe ¹³⁴ , Asp ¹³⁵ , Asn ¹³⁸ , Cys ¹³⁹ , Thr ¹⁴¹ , Asn ⁷⁰⁵ , Ala ⁷⁰⁶ , Ser ⁷⁰⁹ , Thr ⁷¹⁰ , Lys ⁷⁸⁰ , Asn ⁷⁸¹ , Ser ⁷⁸⁴
Oleuropein	Naringen	−8.54	0.55	Tyr ³² , Lys ⁴⁷ , Tyr ¹²⁹ , His ¹³³ , Phe ¹³⁴ , Asp ¹³⁵ , Asn ¹³⁸ , Ser ⁷⁰⁹ , Thr ⁷¹⁰ , Asp ⁷¹¹ , Lys ⁷¹⁴ , Ala ⁷⁷¹ , Ser ⁷⁷² , Gln ⁷⁷³ , Gly ⁷⁷⁴ , Ser ⁷⁷⁸ , Lys ⁷⁸⁰ , Asn ⁷⁸¹ , Ser ⁷⁸⁴
	−8.31	0.81	Tyr ³² , Lys ⁴⁷ , Phe ⁴⁸ , Tyr ¹²⁹ , Ala ¹³⁰ , His ¹³³ , Phe ¹³⁴ , Asp ¹³⁵ , Asn ¹³⁸ , Cys ¹³⁹ , Asp ¹⁴⁰ , Thr ¹⁴¹ , Leu ¹⁴² , Thr ⁷¹⁰ , Asp ⁷¹¹ , Lys ⁷¹⁴ , Ser ⁷⁷⁸ , Lys ⁷⁸⁰ , Asn ⁷⁸¹ , Ser ⁷⁸⁴	

Table 1. Cont.

Target	Phytochemicals	Binding Energy (kcal/mol)	Dissociation Constant (μ M)	Active Site Residue
Spike protein (S)	Glycyrrhizin	−9.49	0.11	Tyr ⁷⁴¹ , Ile ⁷⁴² , Cys ⁷⁴³ , Gly ⁷⁴⁴ , Asp ⁷⁴⁵ , Phe ⁸⁵⁵ , Asn ⁸⁵⁶ , Val ⁹⁶³ , Lys ⁹⁶⁴ , Leu ⁹⁶⁶ , Ser ⁹⁶⁷ , Ser ⁹⁷⁵ , Val ⁹⁷⁶ , Leu ⁹⁷⁷ , Asn ⁹⁷⁸ , Arg ¹⁰⁰⁰
		−9.29	0.16	Val ⁴⁷ , His ⁴⁹ , Lys ³⁰⁴ , Met ⁷⁴⁰ , Tyr ⁷⁴¹ , Ile ⁷⁴² , Cys ⁷⁴³ , Gly ⁷⁴⁴ , Asp ⁷⁴⁵ , Phe ⁸⁵⁵ , Asn ⁸⁵⁶ , Val ⁹⁶³ , Lys ⁹⁶⁴ , Leu ⁹⁶⁶ , Ser ⁹⁶⁷ , Ser ⁹⁷⁵ , Val ⁹⁷⁶ , Leu ⁹⁷⁷ , Asn ⁹⁷⁸ , Arg ¹⁰⁰⁰
	Rhodiolin	−8.68	0.43	Arg ¹⁰² , Gly ¹⁰³ , Trp ¹⁰⁴ , Ile ¹¹⁹ , Asn ¹²¹ , Val ¹²⁶ , Ile ¹²⁸ , Phe ¹⁶⁸ , Tyr ¹⁷⁰ , Ser ¹⁷² , Arg ¹⁹⁰ , Phe ¹⁹² , Ile ²⁰³ , His ²⁰⁷ , Leu ²²⁶ , Val ²²⁷ , Asp ²²⁸ , Leu ²²⁹
	Hesperidin	−8.53	0.56	Tyr ³⁸ , Asp ⁴⁰ , Lys ⁴¹ , Val ⁴² , Phe ⁴³ , Arg ⁴⁴ , Lys ²⁰⁶ , Phe ²²⁰ , Ser ²²¹ , Ala ²²² , Glu ²²⁴ , Pro ²²⁵ , Leu ²²⁶ , Tyr ²⁷⁹ , Gly ²⁸³ , Thr ²⁸⁴
		−8.18	1.01	Asn ⁷¹⁰ , Thr ¹⁰⁷⁶ , Ser ¹⁰⁹⁷ , Gly ¹⁰⁹⁹ , Thr ¹¹⁰⁰ , His ¹¹⁰¹ , Trp ¹¹⁰² , Ile ¹¹¹⁴ , Ile ¹¹¹⁵ , Val ¹¹³³ , Asn ¹¹³⁴ , Asn ¹¹³⁵ , Thr ¹¹³⁶ , Tyr ¹¹³⁸
	Umbelliprenin	−8.12	1.11	Trp ¹⁰⁴ , Ile ¹¹⁹ , Asn ¹²¹ , Val ¹²⁶ , Ile ¹²⁸ , Phe ¹⁶⁸ , Tyr ¹⁷⁰ , Ser ¹⁷² , Arg ¹⁹⁰ , Phe ¹⁹² , Phe ¹⁹⁴ , Ile ²⁰³ , Ser ²⁰⁵ , Lys ²⁰⁶ , His ²⁰⁷ , Leu ²²⁶ , Val ²²⁷ , Leu ²²⁹
	18,β-Glycyrrhetic acid	−8.08	1.2	Tyr ³⁸ , Asp ⁴⁰ , Lys ⁴¹ , Val ⁴² , Phe ⁴³ , Arg ⁴⁴ , Glu ²²⁴ , Pro ²²⁵ , Tyr ²⁷⁹ , Gly ²⁸³
		−7.99	1.38	His ¹¹⁰¹ , Trp ¹¹⁰² , Phe ¹¹⁰³ , Ile ¹¹¹⁴ , Ile ¹¹¹⁵ , Asn ¹¹³⁵ , Thr ¹¹³⁶ , Val ¹¹³⁷ , Tyr ¹¹³⁸ , Asp ¹¹³⁹ , Gln ¹¹⁴² , Pro ¹¹⁴³
	Silyhermin	−8.05	1.25	Arg ³⁵⁵ , Tyr ³⁹⁶ , Pro ⁴²⁶ , Asp ⁴²⁸ , Phe ⁴²⁹ , Thr ⁴³⁰ , Lys ⁴⁶² , Pro ⁴⁶³ , Phe ⁴⁶⁴ , Ser ⁵¹⁴ , Phe ⁵¹⁵ , Glu ⁵¹⁶ , Leu ⁵¹⁷ , Leu ⁵¹⁸
	Ellagic acid	−8.1	1.16	Ser ⁷³⁰ , Met ⁷³¹ , Thr ⁷³² , Lys ⁷³³ , Gln ⁷⁷⁴ , Thr ⁷⁷⁸ , Phe ⁸²³ , Val ⁸⁶⁰ , Leu ⁸⁶¹ , Pro ⁸⁶² , Pro ⁸⁶³ , Asp ⁸⁶⁷ , Ile ⁸⁷⁰ , Ala ¹⁰⁵⁶ , Pro ¹⁰⁵⁷ , His ¹⁰⁵⁸ , Gly ¹⁰⁵⁹
Helicase	Glycyrrhizin	−11.57	0.003	Pro ¹⁷⁵ , Leu ¹⁷⁶ , Asn ¹⁷⁷ , Lys ²⁰² , Leu ⁴⁰⁵ , Pro ⁴⁰⁶ , Ala ⁴⁰⁷ , Pro ⁴⁰⁸ , Arg ⁴⁰⁹ , Leu ⁴¹² , Thr ⁴¹³ , Gly ⁴¹⁵ , Thr ⁴¹⁶ , Leu ⁴¹⁷ , Phe ⁴²² , Ser ⁴⁸⁵ , Ser ⁴⁸⁶ , Pro ⁵¹⁴ , Tyr ⁵¹⁵ , Asn ⁵¹⁶ , Asn ⁵¹⁹ , Thr ⁵³² , Val ⁵³³ , Asp ⁵³⁴ , His ⁵⁵⁴ , Asn ⁵⁵⁷ , Asn ⁵⁵⁹ , Arg ⁵⁶⁰
	18,β-Glycyrrhetic acid	−9.91	0.054	Ala ⁴ , Val ⁶ , Arg ¹⁵ , Arg ²¹ , Arg ²² , Pro ²³ , Phe ²⁴ , Arg ¹²⁹ , Leu ¹³² , Phe ¹³³ , Glu ¹³⁶ , Pro ²³⁴ , Leu ²³⁵ , Ser ²³⁶
	Solophenol A	−9.4	0.13	Pro ¹⁷⁵ , Leu ¹⁷⁶ , Asn ¹⁷⁷ , Arg ¹⁷⁸ , Thr ¹⁹⁹ , Phe ²⁰⁰ , Glu ²⁰¹ , Lys ²⁰² , Gly ²⁰³ , Asp ²⁰⁴ , Val ²¹⁰ , Tyr ²¹¹ , Arg ²¹² , Val ⁴⁸⁴ , Ser ⁴⁸⁶ , Asn ⁵¹⁶ , Ser ⁵¹⁷ , Asn ⁵¹⁹ , Ala ⁵²⁰ , Thr ⁵³⁰ , Thr ⁵³² , Asp ⁵³⁴
	Hesperidin	−8.93	0.283	Lys ¹³⁹ , Glu ¹⁴² , Glu ¹⁴³ , Lys ¹⁴⁶ , Arg ¹⁷⁸ , Asn ¹⁷⁹ , Val ¹⁸¹ , Glu ¹⁹⁷ , Thr ²²⁸ , His ²³⁰ , Cys ³⁰⁹ , Arg ³³⁷ , Arg ³³⁹ , Met ³⁷⁸ , Ala ³⁷⁹ , Thr ³⁸⁰ , Tyr ³⁸² , Asp ³⁸³ , Ala ⁴⁰⁷ , Pro ⁴⁰⁸ , Thr ⁴¹⁰
	Baicalin	−8.9	0.29	Asn ¹⁷⁷ , Arg ¹⁷⁸ , Thr ¹⁹⁹ , Phe ²⁰⁰ , Glu ²⁰¹ , Lys ²⁰² , Arg ²¹² , Asn ⁵¹⁶ , Asn ⁵¹⁹ , Ala ⁵²⁰ , Thr ⁵³⁰ , Gln ⁵³¹ , Thr ⁵³² , Asp ⁵³⁴
	Glycyrrhizin	−10.07	0.04	Arg ⁶¹ , Asn ⁶⁴ , leu ²⁸ , val ²⁹ , leu ³¹ , ala ³² , ile ³³ , ala ³⁶ , arg ³⁸ , Leu ²⁷ , Thr ³⁰ , Leu ³¹ , Leu ³⁴ , Leu ³⁷ , Leu ³⁹ , Tyr ⁴² , Cys ⁴³ , Ile ⁴⁶ , Val ⁴⁷ , Val ⁴⁹ , Ser ⁵⁰ , Leu ⁵¹ , Pro ⁵⁴ , Tyr ⁵⁷
E-channel protein	18,β-Glycyrrhetic acid	−9.72	0.07	Arg ⁶¹ , Leu ²⁸ , Val ²⁹ , Leu ³¹ , Ala ³² , Thr ³⁵ , Leu ²⁷ , Thr ³⁰ , Leu ³¹ , Ile ⁴⁶ , Val ⁴⁷ , Leu ⁵¹ , Pro ⁵⁴ , Tyr ⁵⁷
	Umbelliprenin	−8.90	0.3	Ala ²² , Val ²⁵ , Phe ²⁶ , Leu ²⁸ , Val ²⁹ , Leu ¹⁹ , Phe ²⁰ , Ala ²² , Phe ²³ , Val ²⁴ , Phe ²⁶ , Leu ²⁷ , Asn ⁶⁴ , Leu ⁶⁵
	Euchrestafavanone A	−8.90	0.3	Arg ⁶¹ , Asn ⁶⁴ , dval ²⁵ , dphe ²⁶ , dleu ²⁸ , dval ²⁹ , Ala ²² , Phe ²³ , Phe ²⁶ , Leu ²⁷ , Thr ³⁰ , Leu ³⁴ , Cys ⁴³ , Ile ⁴⁶ , Val ⁴⁷ , Val ⁴⁹ , Ser ⁵⁰ , Leu ⁵¹
	Baicalin	−8.89	0.3	Ala ²² , Val ²⁵ , Phe ²⁶ , Val ²⁹ , Phe ²⁰ , Ala ²² , Phe ²³ , Val ²⁴ , Phe ²⁶ , Leu ²⁷ , Thr ³⁰ , Arg ⁶¹ , Asn ⁶⁴ , Leu ⁶⁵
	Silibinin A	−8.13	1.1	Leu ²⁸ , Leu ³¹ , Ala ³² , Thr ³⁵ , Cys ⁴⁰ , Ile ⁴⁶ , Ser ⁵⁰ , Leu ⁵¹ , Lys ⁵³ , Pro ⁵⁴ , Phe ⁵⁶ , Tyr ⁵⁷ , Tyr ⁵⁹ , Ser ⁶⁰

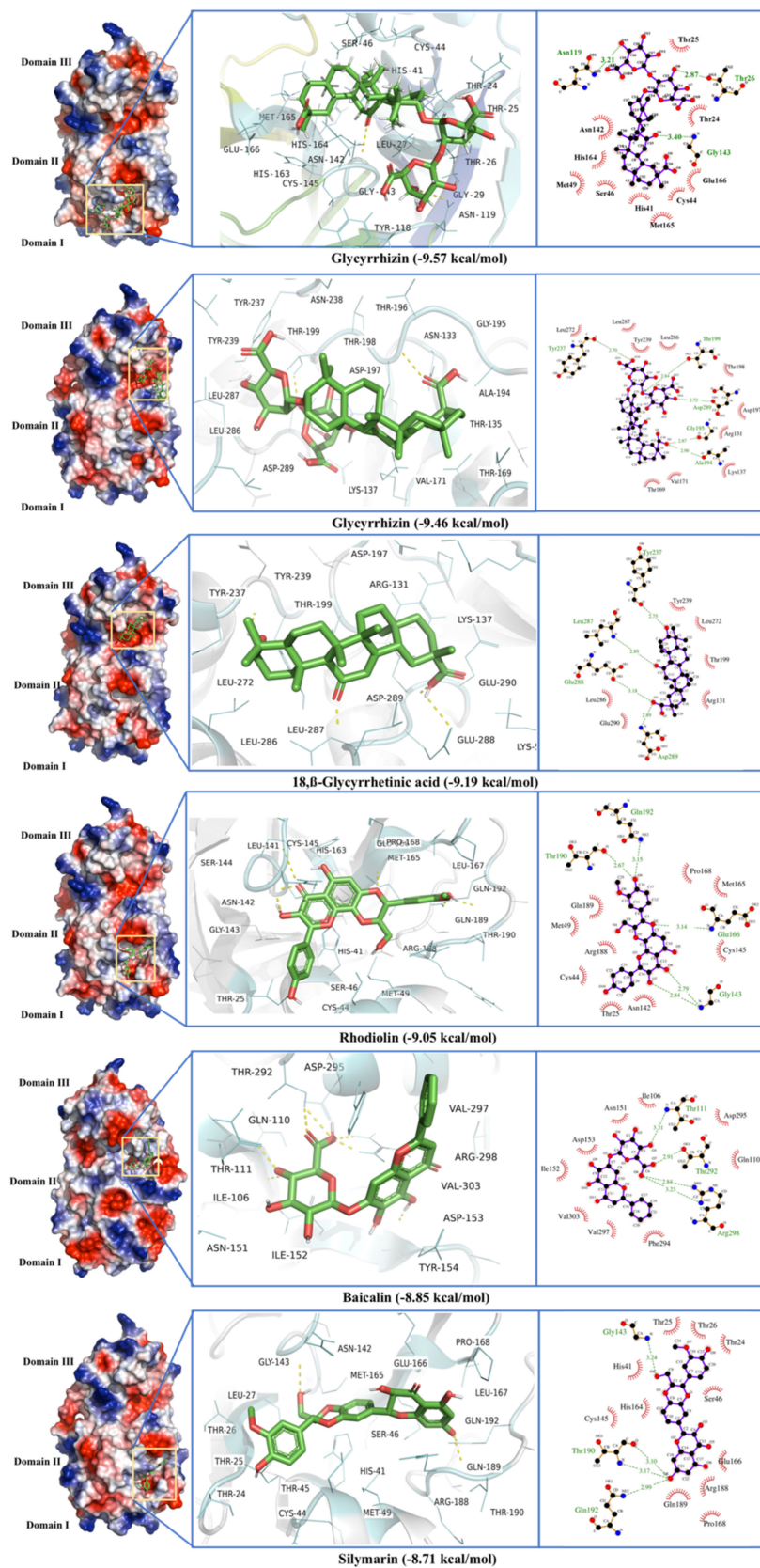


Figure 2. Molecular docking of Glycyrrhizin, 18,β-Glycyrrhetic acid, Rhodiolin, Baicalin, and Silymarin with SARS-CoV-2 main protease (MPro).

The allosteric binding sites for Glycyrrhizin were also found between domains II and III and included the residues Arg¹³¹, Lys¹³⁷, Asp¹⁹⁷, Thr¹⁹⁸, Thr¹⁹⁹, Tyr²³⁹, Leu²⁷¹, Asn²⁷⁴, Gly²⁷⁵, Met²⁷⁶, Asn²⁷⁷, Gly²⁷⁸, Arg²⁷⁹, Ala²⁸⁵, Leu²⁸⁶, Leu²⁸⁷, Glu²⁸⁸, Asp²⁸⁹, and Glu²⁹ where Asp¹⁹⁷, Thr¹⁹⁹, and Ala²⁸⁵ form H-bonds with Glycyrrhizin (Figure 2, Table 1). The Glycyrrhizin binding to this active site may disrupt the native enzyme structure and affects its activity. This distal pocket has also been reported as a promising inhibitor binding site [40,41]. This site consists of both a loop region and β -strands.

The 18, β -Glycyrrhetic acid, a derivative of Glycyrrhizin, showed distal allosteric binding with an energy of $-9.19 \text{ kcal}\cdot\text{mol}^{-1}$ and dissociation constant of $0.35 \mu\text{M}$. The active residues for 18, β -Glycyrrhetic acid include Lys⁵, Arg¹³¹, Lys¹³⁷, Asp¹⁹⁷, Thr¹⁹⁹, Tyr²³⁷, Tyr²³⁹, Leu²⁷², Leu²⁸⁶, Leu²⁸⁷, Glu²⁸⁸, Asp²⁸⁹, and Glu²⁹⁰. Among these residues, Tyr²³⁷, Leu²⁸⁷, Glu²⁸⁸, and Asp²⁸⁹ formed H-bonds (Figure 2, Table 1). Although 18, β -Glycyrrhetic acid does not directly bind to the proposed site of the enzyme, it interacts with the residues which seem present at the dimer interface of the main protease [42] making the binding more interesting to explore (Figure 2).

Other ligands with prominent binding to the main protease include Rhodiolin and silymarin that target the enzyme catalytic site with binding energies of -9.05 and $-8.81 \text{ kcal}\cdot\text{mol}^{-1}$, while the Baicalin binding site includes some of the distal site residues, including Ile¹⁰⁶, Gln¹¹⁰, Thr¹¹¹, Asn¹⁵¹, Ile¹⁵², Asp¹⁵³, Thr²⁹², Phe²⁹⁴, Val²⁹⁷, Arg²⁹⁸, and Val²⁰³ (Figure 2, Table 1). The strong binding of Baicalin to these distal amino acids may reduce the enzyme activity. The worst docking ligands include methyl tridecanoate (binding energy $-4.01 \text{ kcal}\cdot\text{mol}^{-1}$), Margaric acid (binding energy $-3.91 \text{ kcal}\cdot\text{mol}^{-1}$), and docosanoic acid (binding energy $-3.86 \text{ kcal}\cdot\text{mol}^{-1}$) (Table S1).

The initial MD simulation in the case of Glycyrrhizin (active site binding) shows that an equilibrium was achieved after 25 ns, so simulations were limited to 30 ns. The RMSD and RMSF values show the flexible residues in two regions, one from residues Arg⁴⁰-Asp⁵⁶ (Domain I) and from Ile¹³⁶ to Asp¹⁵³ (Domain II) (Figure 3). This shows the ligand interactions with the active site residues of the enzyme. The fluctuations between Tyr²³⁷ and Gly²⁵¹ show that Glycyrrhizin binding to the active site may also induce a conformational change in other parts of the enzyme. This conformational change may be involved in reducing the enzyme activity. The Rhodiolin-M^{Pro} complex showed huge fluctuation around Ile²⁸¹ to Val²⁹⁶ while minor fluctuations in a loop region around Val⁹¹ to Pro⁹⁶ (Figure 3). The radius of gyration (R) at the end of the MD simulation shows the compactness and stability of the Glycyrrhizin- and rhodiolin-enzyme complexes (Figure S1).

2.2. Papain-Like Protease

Like the M^{Pro}, Papain-like Protease is involved in diverse functions that make it a potential drug target [2]. The ligands with the best docking with PL^{Pro} are listed in Table 1. Most of the ligands indirectly interacted with the active site triad Cys¹¹¹, His²⁷², and Asp²⁸⁶ [43] by binding around the enzyme active site (Figure 4). These triad residues are involved in enzyme activity [43]. Baicalin showed a strong binding with the binding energy of $10.82 \text{ kcal}\cdot\text{mol}^{-1}$ with a dissociation constant of 10 nM . The low dissociation constant shows strong ligand binding even at low concentrations. The active site residues include Arg¹⁶⁶, Ser¹⁷⁰, Val²⁰², Glu²⁰³, Met²⁰⁶, Tyr²⁰⁷, Met²⁰⁸, Cys¹⁵⁵, Asn¹⁵⁶, Lys¹⁵⁷, Glu¹⁶¹, Leu¹⁶², Gly¹⁶³, Asp¹⁶⁴, Val¹⁶⁵, Glu¹⁶⁷, Tyr¹⁷¹, Pro²⁴⁸, Tyr²⁶⁴, Tyr²⁶⁸, Gln²⁶⁹, and Tyr²⁷³ (Figure 4). Baicalin shows π - π interactions with Tyr²⁶⁸, while H-bonding is observed with Cys¹⁵⁵, Ly¹⁵⁷, and Tyr¹⁷¹ (Figure 4). Previously, a binding site in crystal structure of papain-like protease (PL^{Pro}) (PDB ID 6WX4) was defined by the residues; Trp¹⁰⁶, Asn¹⁰⁹, Tyr¹¹², Cys¹¹¹, Leu¹⁶², Asp¹⁶⁴, Val¹⁶⁵, Arg¹⁶⁶, Me²⁰⁸, Pro²⁴⁷, Pro²⁴⁸, Tyr²⁶⁴, Gln²⁶⁹, Cys²⁷⁰, Gly²⁷¹, His²⁷², Tyr²⁷³, and Thr³⁰¹ [44]. This shows although Biacalin does not directly interact with the catalytic triad, it binds in the vicinity of the enzyme active site very strongly and impairs its proper functioning.

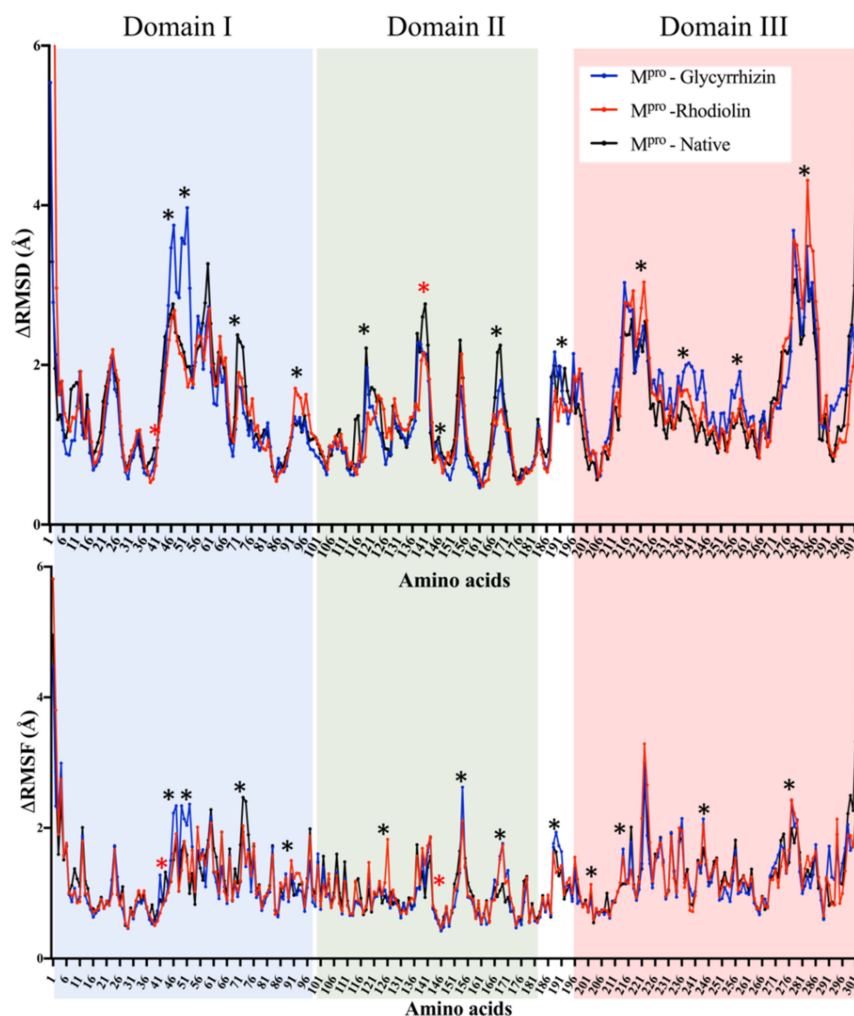


Figure 3. RMSD and RMSF calculated from 30 ns molecular dynamics simulation of Glycyrrhizin (blue) and Rhodiolin (red) docked with SARS-CoV-2 main protease (MPro). The residues with dynamic RMSD and RMSF are mentioned with '*' while red '*' shows the active site residues.

Hesperidin showed the second-best docking with PL^{Pro} with a binding energy of $-10.61 \text{ kcal.mol}^{-1}$ and a dissociation constant of $0.02 \mu\text{M}$. The active site residues include Arg¹⁸³, Leu¹⁸⁵, Leu¹⁹⁹, Glu²⁰³, Met²⁰⁶, Tyr²⁰⁷, Met²⁰⁸, Gly²⁰⁹, Phe²¹⁶, Val²²⁰, Gln²²¹, Ile²²², Pro²²³, Lys²³², Lys¹⁵⁷, Thr¹⁵⁸, Glu¹⁶¹, Leu¹⁶², Gly¹⁶³, Asp¹⁶⁴, Val¹⁶⁵, Glu¹⁶⁷, Pro²⁴⁸, Tyr²⁶⁴, Tyr²⁶⁸, Gln²⁶⁹, Cys²⁷⁰, Tyr²⁷³, and Thr³⁰¹. Among these active site residues, Lys¹⁵⁷, Tyr²⁰⁷, Met²⁰⁸, and Lys²³² formed H-bond with Hesperidin (Figure 4). Lys¹⁵⁷, Arg¹⁶⁶, and Tyr²⁶⁸ seem to be involved in all top five ligand-enzyme interactions.

The worst docking ligands include 6,9,12-octadecatrienoic acid (binding energy $-4.85 \text{ kcal.mol}^{-1}$), docosanoic acid (binding energy $-4.64 \text{ kcal.mol}^{-1}$), and acetoxyhydroamic acid (binding energy $-4.13 \text{ kcal.mol}^{-1}$). These compounds were unable to bind the proposed active site (Table S1).

MD simulations of 30 ns were run for Baicalin, Hesperidin, and Solophenol, where considerable RMSD and RMSF fluctuations were found in the active site residues of PL^{Pro} (Figure 5). In the case of Baicalin, strong binding and low dissociation constant for the Baicalin-enzyme complex is also confirmed by MD simulations. N-terminal region from Val²¹ to Pro⁴⁶ is the most flexible region, while regions including Tyr⁷¹ to Asp⁷⁶, Leu¹⁰¹ to Gln¹²¹, Gly²⁶⁶ to Ile²⁷⁶, and Thr²⁸¹ to Lys²⁹² seem to be involved in Baicalin-PL^{Pro} interactions (Figure 5). The Hesperidin-enzyme complex Radius of gyration (R_g) for

Solophenol increased in 15–30 ns of MD simulation but Baicalin and Hesperidin, due to strong binding, show the R_g similar to the native enzyme (Figure S2).

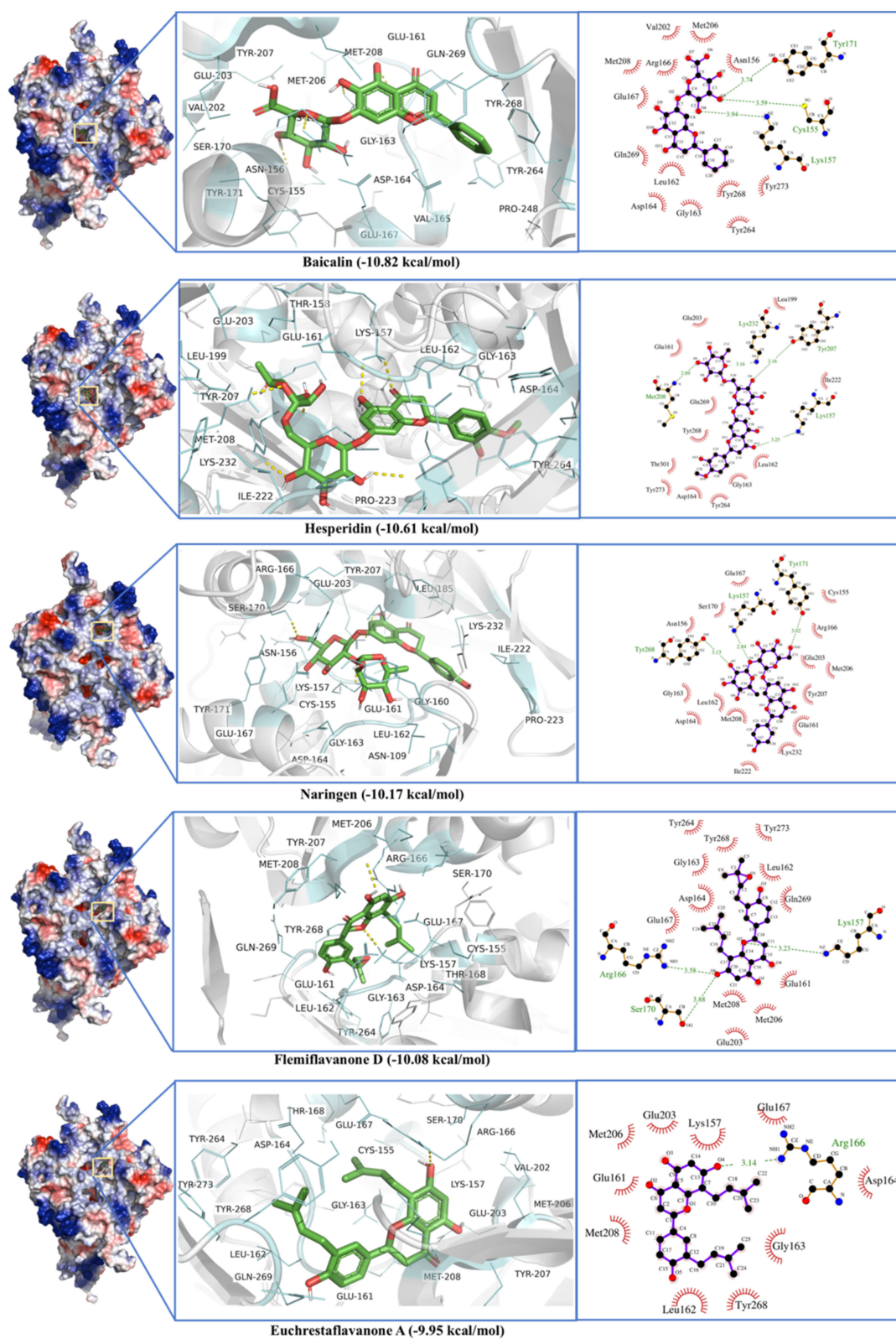


Figure 4. Molecular docking of Baicalin, Hesperidin, Solophenol, Naringin, Flemiflavanone D, and Euchrestaflavanone A against SARS-CoV-2 papain-like protease (PL^{Pro}).

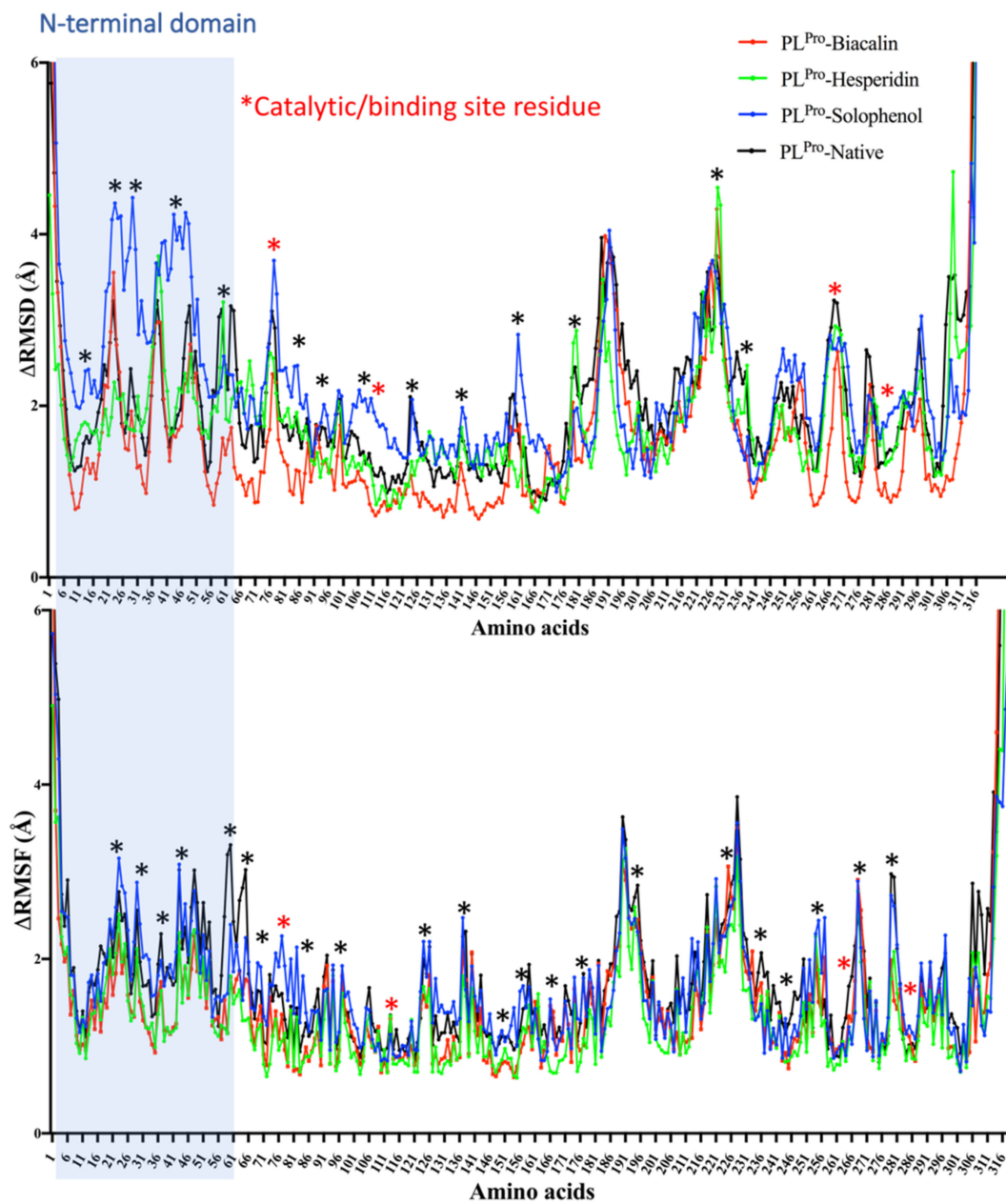


Figure 5. RMSD and RMSF calculated from a 30 ns molecular dynamics simulation of Baicalin (red), Hesperidin (green), and Solophenol (blue) docked with SARS-CoV-2 PL^{Pro}. The residues with dynamic RMSD and RMSF are mentioned with '*' while red '*' shows the active site residues.

2.3. RNA-Dependent RNA Polymerase (RdRp)

The RNA-dependent RNA Polymerase (RdRp), the main replication enzyme for SARS-CoV-2, was screened against a library of phytochemicals (Table S1). Glycyrrhizin showed the strongest binding to RdRp. Interestingly, Glycyrrhizin strongly interacts with RdRp at two different binding sites with binding energies of -10.27 and -9.96 kcal·mol⁻¹ with dissociation constants of 0.03 and 0.05 μ M (Table 1, Figure 6). The key residues of the Glycyrrhizin-enzyme complex include Asp⁴⁵², Tyr⁴⁵⁵, Lys⁵⁵¹, Arg⁵⁵³, Ala⁵⁵⁴, Arg⁵⁵⁵, Thr⁵⁵⁶, Trp⁶¹⁷, Asp⁶¹⁸, Tyr⁶¹⁹, Pro⁶²⁰, Lys⁶²¹, Cys⁶²², Asp⁶²³, Arg⁶²⁴, Ser⁷⁵⁹, Asp⁷⁶⁰, Asp⁷⁶¹, Ala⁷⁶², Lys⁷⁹⁸, Cys⁷⁹⁹, Trp⁸⁰⁰, Glu⁸¹¹, Phe⁸¹², Cys⁸¹³, Ser⁸¹⁴, where Asp⁴⁵², Ala⁵⁵⁴, Trp⁶¹⁷, Asp⁷⁶⁰, Lys⁷⁹⁸, Glu⁸¹¹, Cys⁸¹³, and Ser⁸¹⁴ are involved in H-binding (Figure 6). The formation of multiple H-bonds stabilizes the Glycyrrhizin-RdRp interactions.

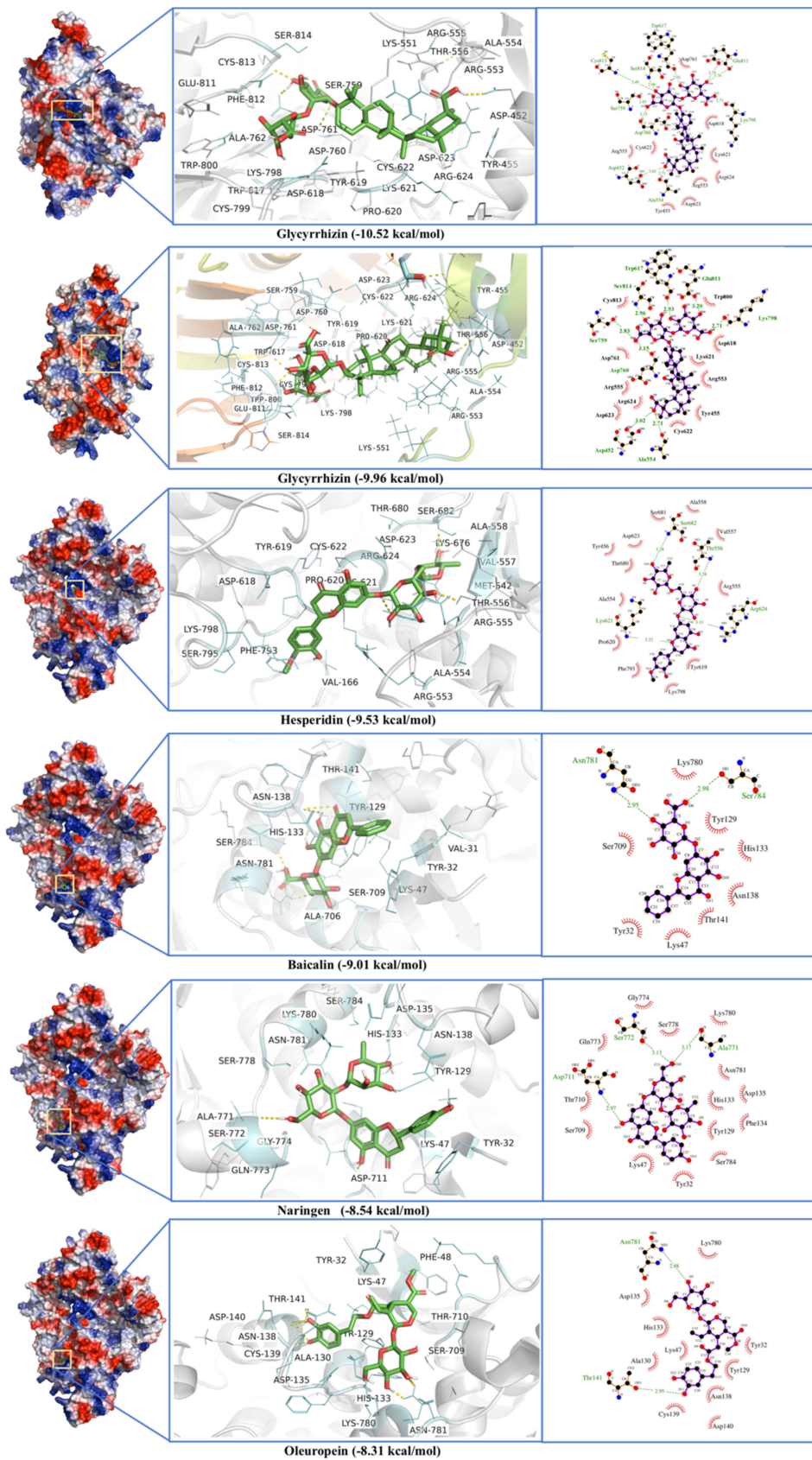


Figure 6. Glycyrrhizin, Hesperidin, Baicalin, Naringen, and Oleuropein docking against SARS-CoV-2 RNA-dependent RNA polymerase (RdRp).

The second binding site for Glycyrrhizin includes the residues; Ala⁴⁶, Lys⁴⁷, Tyr¹²⁹, His¹³³, Phe¹³⁴, Asp¹³⁵, Met⁶¹⁵, Ser⁷⁰⁹, Thr⁷¹⁰, Asp⁷¹¹, Phe⁷⁶⁶, Ala⁷⁷¹, Ser⁷², Gln⁷⁷³, Gly⁷⁷⁴, Ser⁷⁷⁸, Ile⁷⁷⁹, Lys⁷⁸⁰, Asn⁷⁸¹, Ser⁷⁸⁴, and Thr⁸⁰¹. Among these residues, Tyr¹²⁹, His¹³³, Ser⁷⁰⁹, Asp⁷¹¹, and Asn⁷⁸¹ form H-bonds (Figure 6). The binding site of RNA-dependent RNA Polymerase (RdRp) has already been defined by using cryo-EM structures [45] where key catalytic site residues are Lys⁵⁰⁰, Ser⁵⁰¹, Asn⁵⁰⁷, Lys⁵⁴⁵, Arg⁵⁵⁵, Asp⁶¹⁸, Ser⁷⁵⁹, Asp⁷⁶⁰, Asp⁷⁶¹, Cys⁸¹³, Ser⁸¹⁴, and Gln⁸¹⁵. It seems that Glycyrrhizin interacts with these residues with a high binding affinity (multiple H-bonds) and may impair the RdRp interactions with the RNA.

Hesperidin, though not interacting with the proposed RdRp active site, binds near to the enzyme active site, where Thr⁵⁵⁶, Lys⁶²¹, Arg⁶²⁴, and Ser⁶²⁸ form H-bonds and Phe⁷⁹³ shows π - π interactions. Hesperidin showed a binding energy of -9.53 kcal·mol⁻¹ and with a dissociation constant of 0.1 μ M. Baicalin, Naringen, and Oleuropein bind to a completely different site in RdRp, where Thr¹⁴¹, Asn⁷⁸¹, and Ser⁷⁸⁴ are key residues (Figure 6). Baicalin showed the best binding energy of -9.01 kcal·mol⁻¹ with a dissociation constant of 0.12 μ M. Active site residues are Phe³⁵, Asp³⁶, Ile³⁷, Tyr³⁸, Asn³⁹, Phe⁴⁸, Leu⁴⁹, Lys⁵⁰, Thr⁵¹, Asn⁵², Val²⁰⁴, Thr²⁰⁶, Asp²⁰⁸, Asn²⁰⁹, Asp²¹⁸, Asp²²¹, Tyr⁷²⁸. Among these residues, Tyr³⁸, Asn²⁰⁹, Asp²¹⁸, and Tyr⁷²⁸ formed H-bond (Figure 6).

The worst binders include 11-eicosenoic acid (binding energy -4.11 kcal·mol⁻¹), Oleic acid (binding energy -3.95 kcal·mol⁻¹), and heneicosanoic acid (binding energy -3.76 kcal·mol⁻¹) (Table S1).

A 20 ns MD simulation validates the Glycyrrhizin, Hesperidin, and baicalin interactions with RdRp. Glycyrrhizin and Baicalin show RMSD changes in the interface region consisting of residue from Val²⁵⁸ to Leu²⁷⁰, in the finger region Asp⁴⁸¹ to Tyr⁵¹⁵, Thr⁷³⁸ to Tyr⁷⁷⁰ (Figure 7). The RMSD and RMSF fluctuations seem larger in Baicalin in comparison to Glycyrrhizin and Hesperidin. In the thumb region, substantial RMSD changes were observed in all three complexes. All three ligand-enzyme complexes seem more stable in terms of potential energy than native enzymes (Figure S3).

2.4. Spike Glycoprotein

The phytochemical ligands were screened against Spike Glycoprotein's with both open and closed states of the protein. The ligands with the best docking for spike glycoprotein are listed in Table 1. Glycyrrhizin showed the best binding energy of -9.29 and -9.49 kcal·mol⁻¹ and a dissociation constant of 0.16 and 0.11 μ M for the open and close state of spike glycoproteins, respectively. The active site residues for the open state include Val⁴⁷, His⁴⁹, Lys³⁰⁴, Met⁷⁴⁰, Tyr⁷⁴¹, Ile⁷⁴², Cys⁷⁴³, Gly⁷⁴⁴, Asp⁷⁴⁵, Phe⁸⁵⁵, Asn⁸⁵⁶, Val⁹⁶³, Lys⁹⁶⁴, Leu⁹⁶⁶, Ser⁹⁶⁷, Ser⁹⁷⁵, Val⁹⁷⁶, Leu⁹⁷⁷, Asn⁹⁷⁸, and Arg¹⁰⁰⁰. H-bonds and π - π interactions were observed in the Glycyrrhizin-Spike protein interactions that show strong binding of the ligand. Among these residues of the active site, Gly⁷⁴⁴, Asp⁷⁴⁵, and Arg¹⁰⁰⁰ formed H-bonds, and Tyr⁷⁴¹, Phe⁸⁵⁵ show π - π interactions in an open protein state (Figure 8a). Glycyrrhizin interacts with Tyr⁷⁴¹, Ile⁷⁴², Cys⁷⁴³, Gly⁷⁴⁴, Asp⁷⁴⁵, Phe⁸⁵⁵, Asn⁸⁵⁶, Val⁹⁶³, Lys⁹⁶⁴, Leu⁹⁶⁶, Ser⁹⁶⁷, Ser⁹⁷⁵, Val⁹⁷⁶, Leu⁹⁷⁷, Asn⁹⁷⁸, and Arg¹⁰⁰⁰ residues in the close spike protein state, while Tyr⁷⁴¹, Gly⁷⁴⁴, Asp⁷⁴⁵, and Arg¹⁰⁰⁰ formed H-bonds in the closed state of spike glycoprotein (Figure 8b). This shows Glycyrrhizin's interactions with the S2 subunit of the spike protein.

Rhodiolin and Hesperidin bind to the N-terminal domain of spike protein and show the second-best binding energies, i.e., -8.68 and -8.53 kcal·mol⁻¹ and dissociation constants, i.e., 0.43 and 0.56 μ M for open and states, respectively. Active site residues for Rhodiolin were Arg¹⁰², Gly¹⁰³, Trp¹⁰⁴, Ile¹¹⁹, Asn¹²¹, Val¹²⁶, Ile¹²⁸, Phe¹⁶⁸, Tyr¹⁷⁰, Ser¹⁷², Arg¹⁹⁰, Phe¹⁹², Ile²⁰³, His²⁰⁷, Leu²²⁶, Val²²⁷, Asp²²⁸, Leu²²⁹, where Arg¹⁰² and Asn¹²¹ formed H-bonds (Figure 8a). Hesperidin shows interactions with residues, i.e., Tyr³⁸, Asp⁴⁰, Lys⁴¹, Val⁴², Phe⁴³, Arg⁴⁴, Lys²⁰⁶, Phe²²⁰, Ser²²¹, Ala²²², Glu²²⁴, Pro²²⁵, Leu²²⁶, Tyr²⁷⁹, Gly²⁸³, and Thr²⁸⁴, where Ala²²² forms a H-bond (Figure 8b).

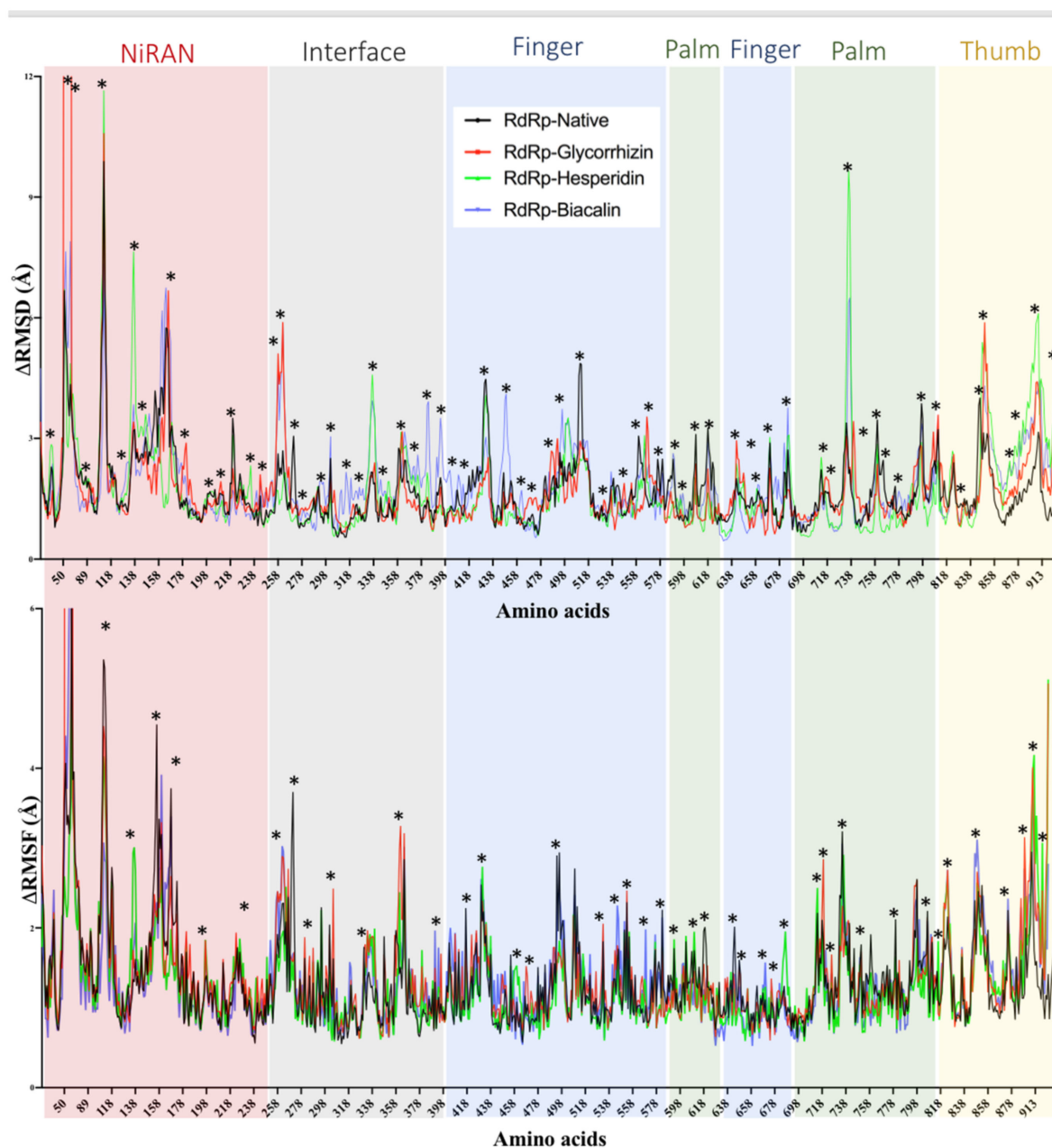
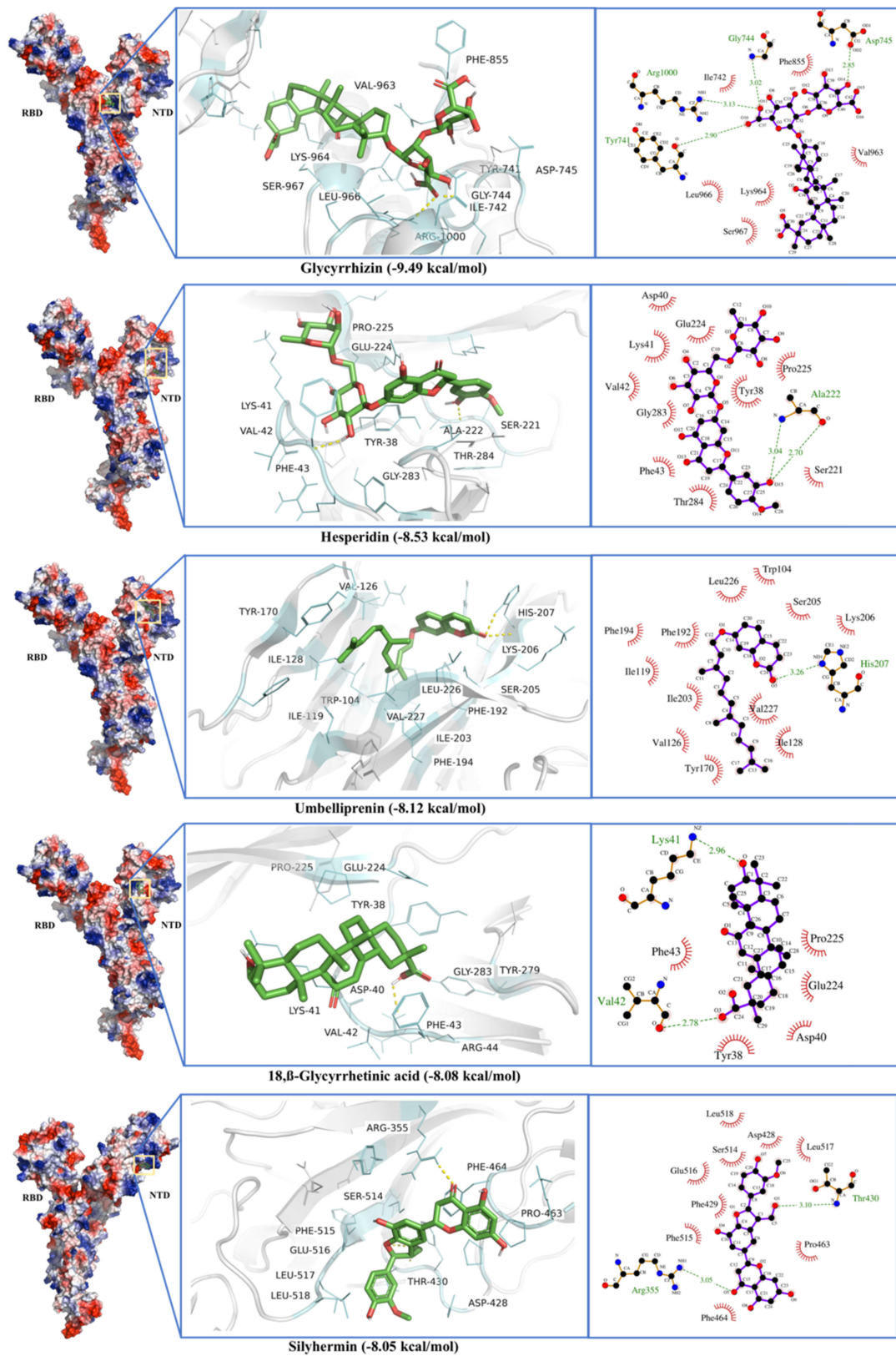


Figure 7. RMSD and RMSF calculated from molecular dynamics simulation of Glycyrrhizin (red), Hesperidin (green), Baicalin (blue) in complex with SARS-CoV-2 RdRp. The residues with dynamic RMSD and RMSF are mentioned with ‘*’.

The worst docking ligands include stearic acid (binding energy $-3.38 \text{ kcal}\cdot\text{mol}^{-1}$), oleic acid (binding energy $-3.26 \text{ kcal}\cdot\text{mol}^{-1}$), and docosanoic acid (binding energy $-3.21 \text{ kcal}\cdot\text{mol}^{-1}$) for open state spike glycoprotein (Table S1). The worst docking ligands include Nervonic acid (binding energy $-3.92 \text{ kcal}\cdot\text{mol}^{-1}$), octadec-9-enyl icosanoate (binding energy $-3.87 \text{ kcal}\cdot\text{mol}^{-1}$), and Tetracosanoic acid (binding energy $-3.71 \text{ kcal}\cdot\text{mol}^{-1}$) for close state spike glycoprotein (Table S1).

MD simulation with a closed state of spike protein shows that Glycyrrhizin-enzyme complexes are more stable than Hesperidin-enzyme complexes in terms of potential energy and R_g (Figure S4). RMSD and RMSF fluctuations in N-terminal domain subunit 1 validate the hesperidin interactions with the residue present in this region (Figure 9). Glycyrrhizin and Hesperidin also show large fluctuations in the S2 areas of spike protein (729–769 and 955–1035 a.a).



(a)

Figure 8. Cont.

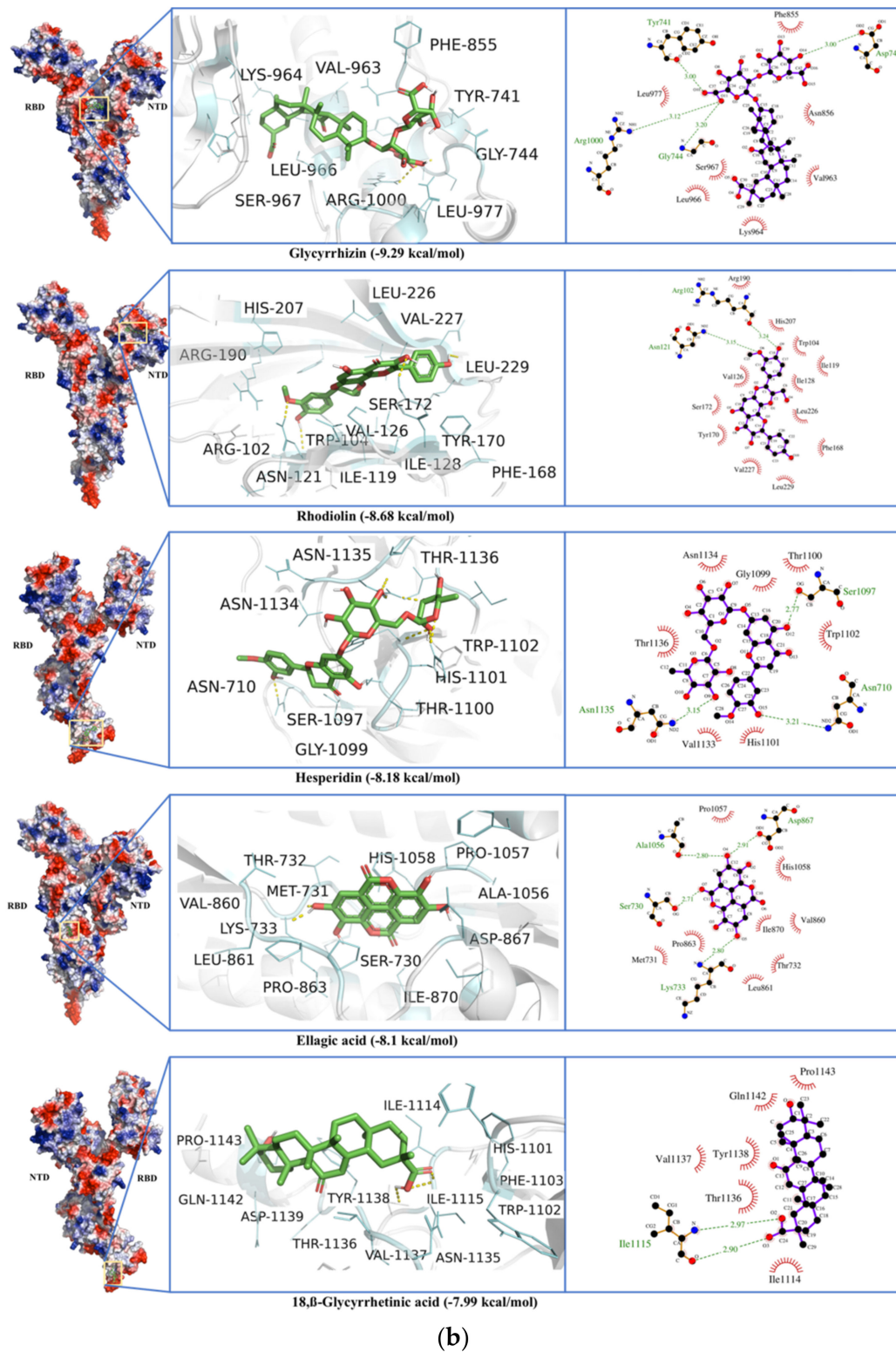


Figure 8. (a) Glycyrrhizin, Rhodioliol, Hesperidin, Ellagic acid, and 18,β-Glycyrrhetic Acid docking to open state of the spike protein of SARS-CoV-2 Spike protein (S). (b) Glycyrrhizin, Hesperidin, Umbelliprenin, 18, β-Glycyrrhetic Acid, and Silyhermin docking to the closed state of the spike protein of SARS-CoV-2 Spike protein (S).

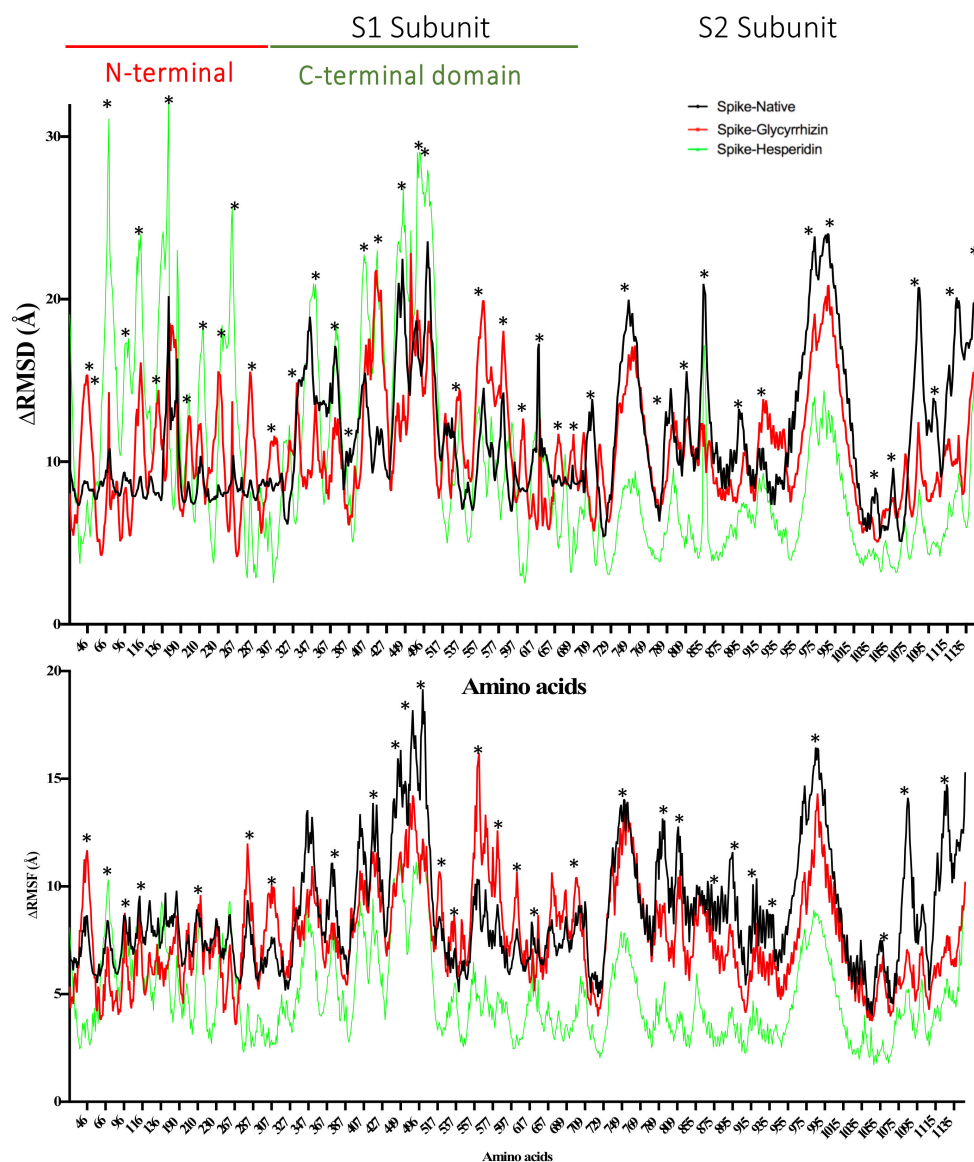


Figure 9. RMSD and RMSF calculated from 30 ns molecular dynamics simulation of Glycyrrhizin (red) and Hesperidin (green) in complex with SARS-CoV-2 spike protein (closed state). The residues with dynamic RMSD and RMSF are mentioned with ‘*’.

2.5. Helicase (Nsp13) Protein

Phytochemicals ligands were docked against Helicase (Nsp13) protein and Glycyrrhizin, β -Glycyrrhetic Acid, Solophenol A, Hesperidin, and Baicalin were found to be the best docking ligands (Table 1). Interestingly, Glycyrrhizin showed very strong interactions with the helicase with a binding energy of $-11.57 \text{ kcal}\cdot\text{mol}^{-1}$ and a dissociation constant of 3 nM. Active site residues are Pro¹⁷⁵, Leu¹⁷⁶, Asn¹⁷⁷, Lys²⁰², Leu⁴⁰⁵, Pro⁴⁰⁶, Ala⁴⁰⁷, Pro⁴⁰⁸, Arg⁴⁰⁹, Leu⁴¹², Thr⁴¹³, Gly⁴¹⁵, Thr⁴¹⁶, Leu⁴¹⁷, Phe⁴²², Ser⁴⁸⁵, Ser⁴⁸⁶, Pro⁵¹⁴, Tyr⁵¹⁵, Asn⁵¹⁶, Asn⁵¹⁹, Thr⁵³², Val⁵³³, Asp⁵³⁴, His⁵⁵⁴, Asn⁵⁵⁷, Asn⁵⁵⁹, and Arg⁵⁶⁰. Among active site six residues, including Asn¹⁷⁷, Lys²⁰², Ser⁴⁸⁵, Asn⁵¹⁶, Asp⁵³⁴, and Arg⁵⁶⁰ form H-bond (Figure 10). Allosteric binding for Glycyrrhizin was observed in a region between RecA1 and RecA2 domains. The same was found to be true in the case of MD simulation, where fluctuations in RMSF and RMSD were observed in a region between RecA1 and RecA2 (Figure 11). The Glycyrrhizin derivative, 18, β -Glycyrrhetic acid, also showed strong interactions with the second-best binding energy of $-9.91 \text{ kcal}\cdot\text{mol}^{-1}$ and a dissociation constant of 54 nM. The active site residues are Ala⁴, Val⁶, Arg¹⁵, Arg²¹, Arg²², Pro²³,

Phe²⁴, Arg¹²⁹, Leu¹³², Phe¹³³, Glu¹³⁶, Pro²³⁴, Leu²³⁵, and Ser²³⁶. Among active site residues, Arg¹⁵ formed two H-bond. Hesperidin shows the binding energy of $-8.93 \text{ kcal}\cdot\text{mol}^{-1}$ binds to enzyme active site where three H-bonds were observed for Lys¹⁴⁶, His²³⁰, and Arg³³⁹ (Figure 10). The worst docking ligands include octadec-9-enyl icosanoat (binding energy $-4.30 \text{ kcal}\cdot\text{mol}^{-1}$), docosanoic acid (binding energy $-4.16 \text{ kcal}\cdot\text{mol}^{-1}$), and aceto-hydroxamic acid (binding energy $-4.11 \text{ kcal}\cdot\text{mol}^{-1}$) for open state spike glycoprotein. Some of these compounds were even unable to bind the proposed active site (Table S1).

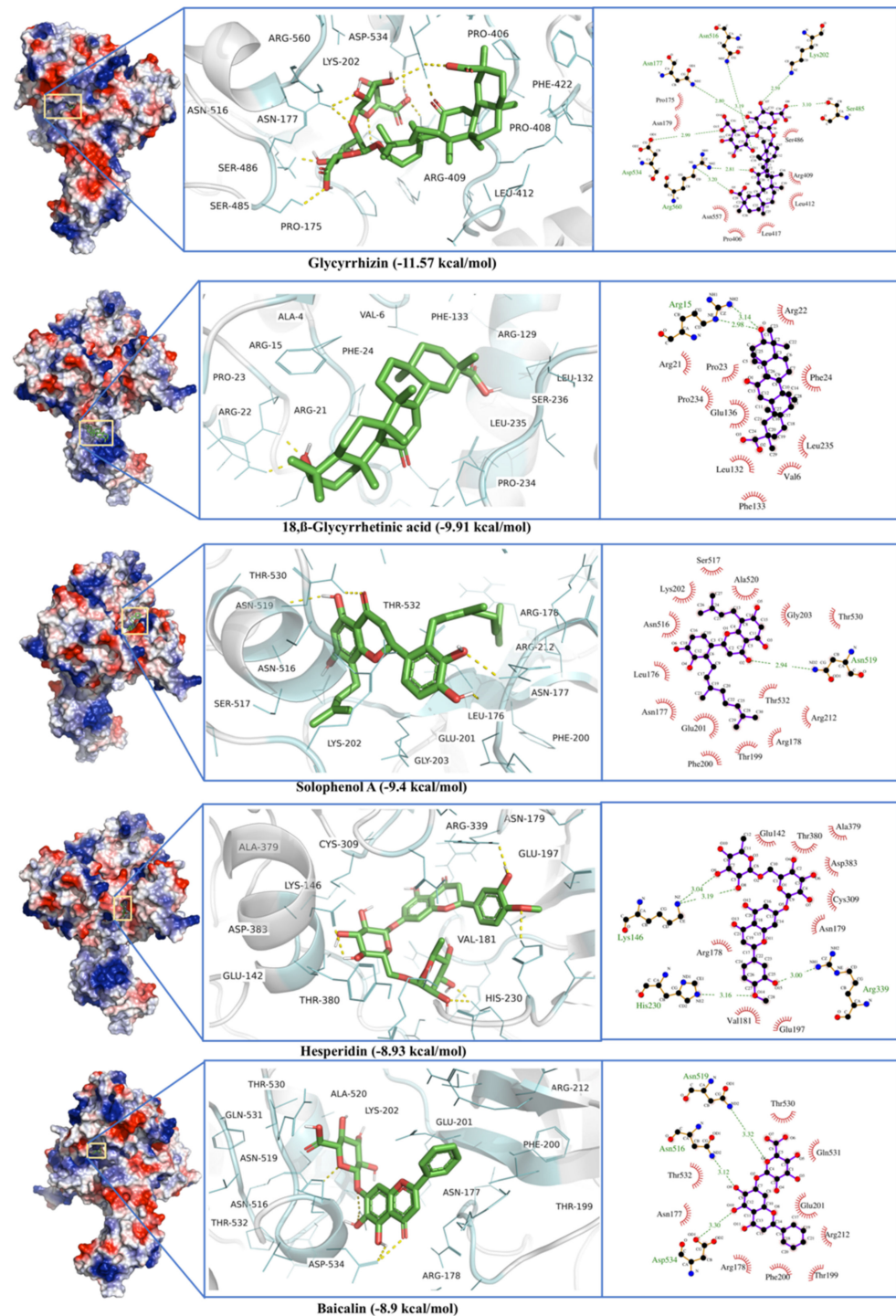


Figure 10. Glycyrrhizin, β-Glycyrrhetic Acid, Solophenol A, Hesperidin, and Baicalin docking to helicase of SARS-CoV-2 Spike protein (S).

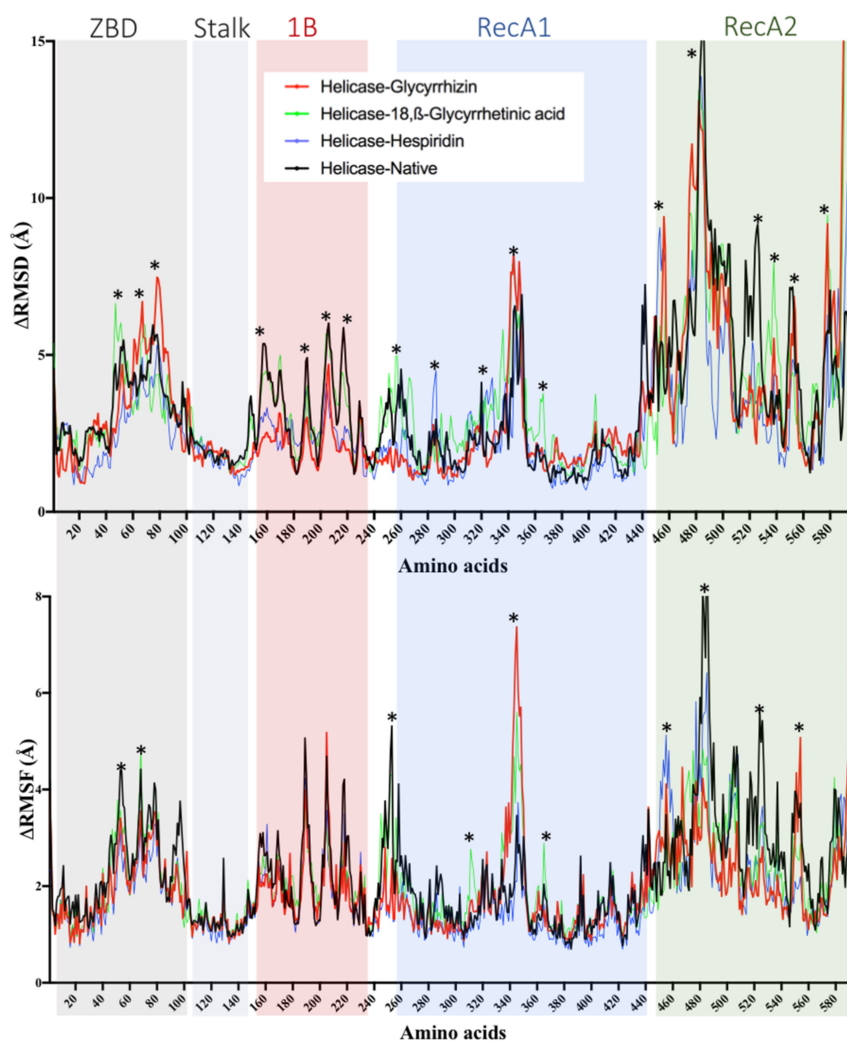


Figure 11. RMSD and RMSF calculated from 30 ns molecular dynamics simulation of Glycyrrhizin (red), Hesperidin (green), Baicalin (blue) in complex with SARS-CoV-2 RdRp. The residues with dynamic RMSD and RMSF are mentioned with '*'.

2.6. E-Channel (Envelope Small Membrane Protein)

The phytochemical ligands were docked against E-channel protein are listed in Table 1. Glycyrrhizin showed the best binding score of $-10.07 \text{ kcal}\cdot\text{mol}^{-1}$ and dissociation constant of $0.04 \mu\text{M}$. Glycyrrhizin interacts with the active site residues present in different chains including Arg⁶¹, and Asn⁶⁴ from Chain A, Leu²⁸, Val²⁹, Leu³¹, Ala³², Ile³³, Ala³⁶, and Arg³⁸ from Chain D, Leu²⁷, Thr³⁰, Leu³¹, Leu³⁴, Leu³⁷, Leu³⁹, Tyr⁴², Cys⁴³, Ile⁴⁶, Val⁴⁷, Val⁴⁹, Ser⁵⁰, Leu⁵¹, Pro⁵⁴, and Tyr⁵⁷ from Chain E. Among these active site residues, Leu²⁸ and Ile⁴⁶ formed H-bonds (Figure 12). 18,β-Glycyrrhetic acid showed the second-best bind energy of $-9.72 \text{ kcal}\cdot\text{mol}^{-1}$ with a dissociation constant of $0.07 \mu\text{M}$. Active site residues are Arg⁶¹ (Chain A), Leu²⁸, Val²⁹, Leu³¹, Ala³², and Thr³⁵ (Chain D), Leu²⁷, Thr³⁰, Leu³¹, Ile⁴⁶, Val⁴⁷, Leu⁵¹, Pro⁵⁴, and Tyr⁵⁷ of Chain E. Among active residues, Arg⁶¹ formed two H-bonds (Figure 12). The worst docking ligands include malic acid (binding energy $-4.05 \text{ kcal}\cdot\text{mol}^{-1}$), oxalic acid (binding energy $-3.24 \text{ kcal}\cdot\text{mol}^{-1}$), and acetoxyhydroxamic acid (binding energy $-3.10 \text{ kcal}\cdot\text{mol}^{-1}$) for open state spike glycoprotein. Some of these compounds were even unable to bind the proposed active site (Table S1).

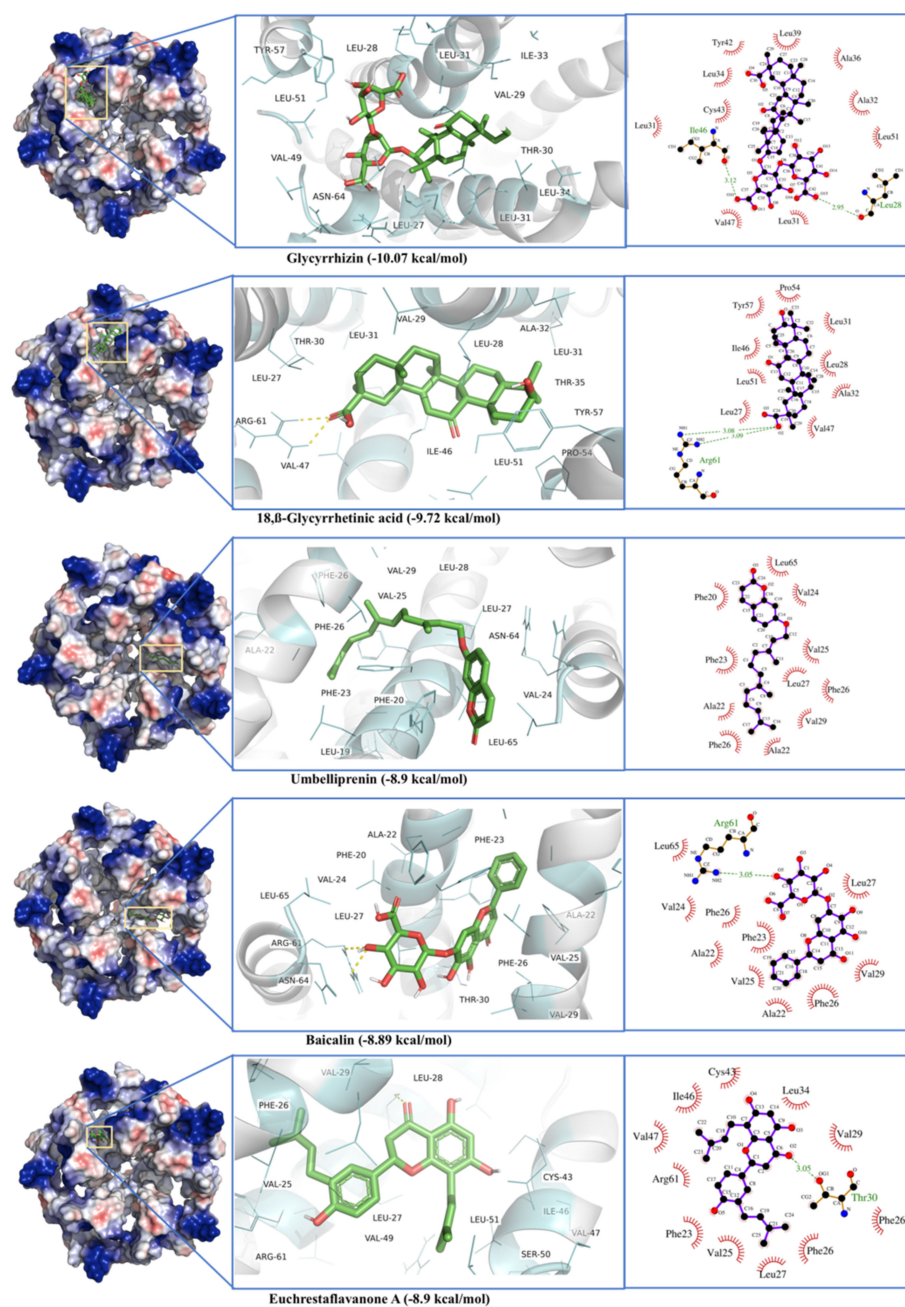
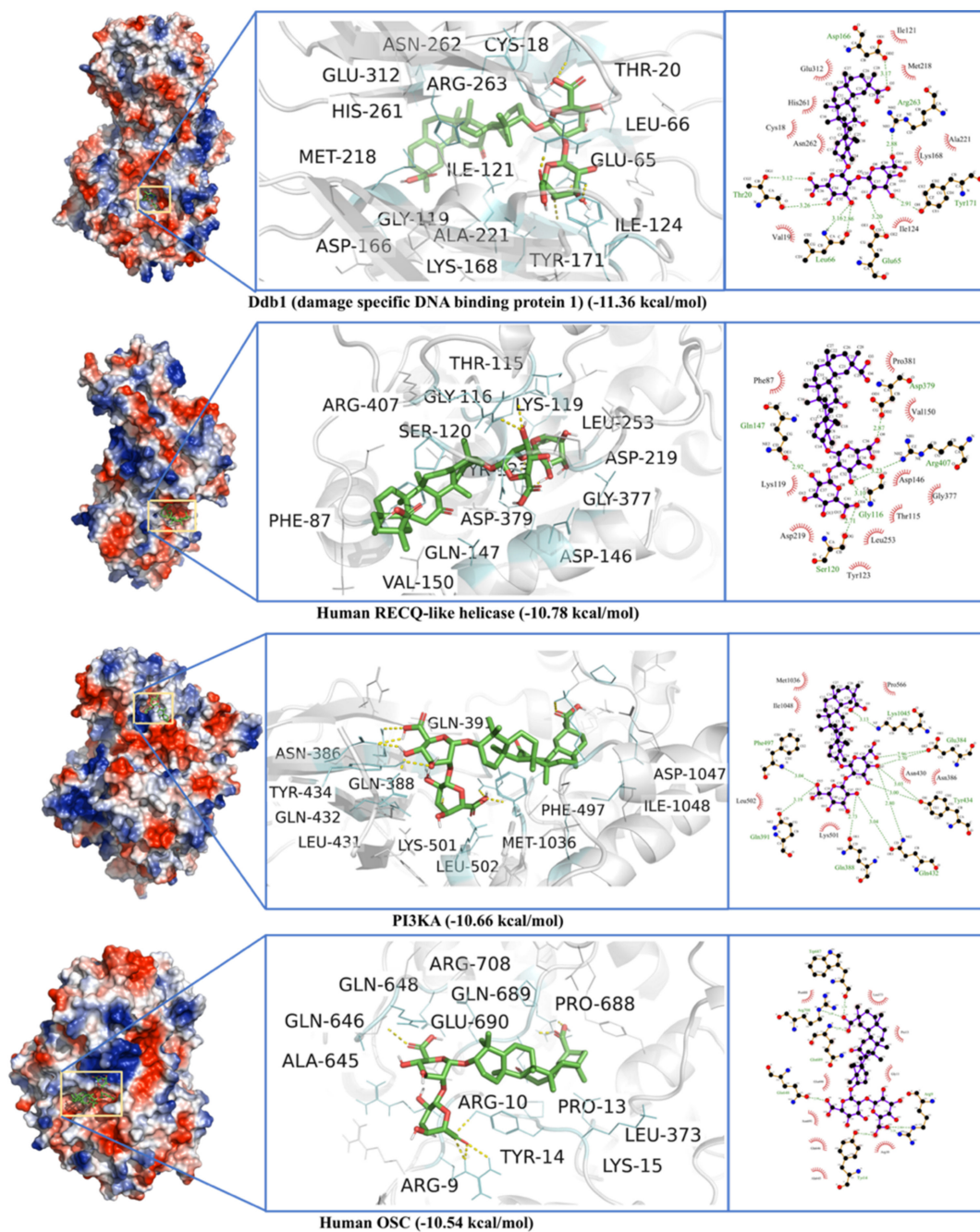


Figure 12. Glycyrrhizin, β -Glycyrrhetic Acid, Solophenol A, Hesperidin, and Baicalin docking to helicase of SARS-CoV-2 Spike protein (S).

2.7. Non-Specific Interactions of Selected Ligands against Human Blood Proteins

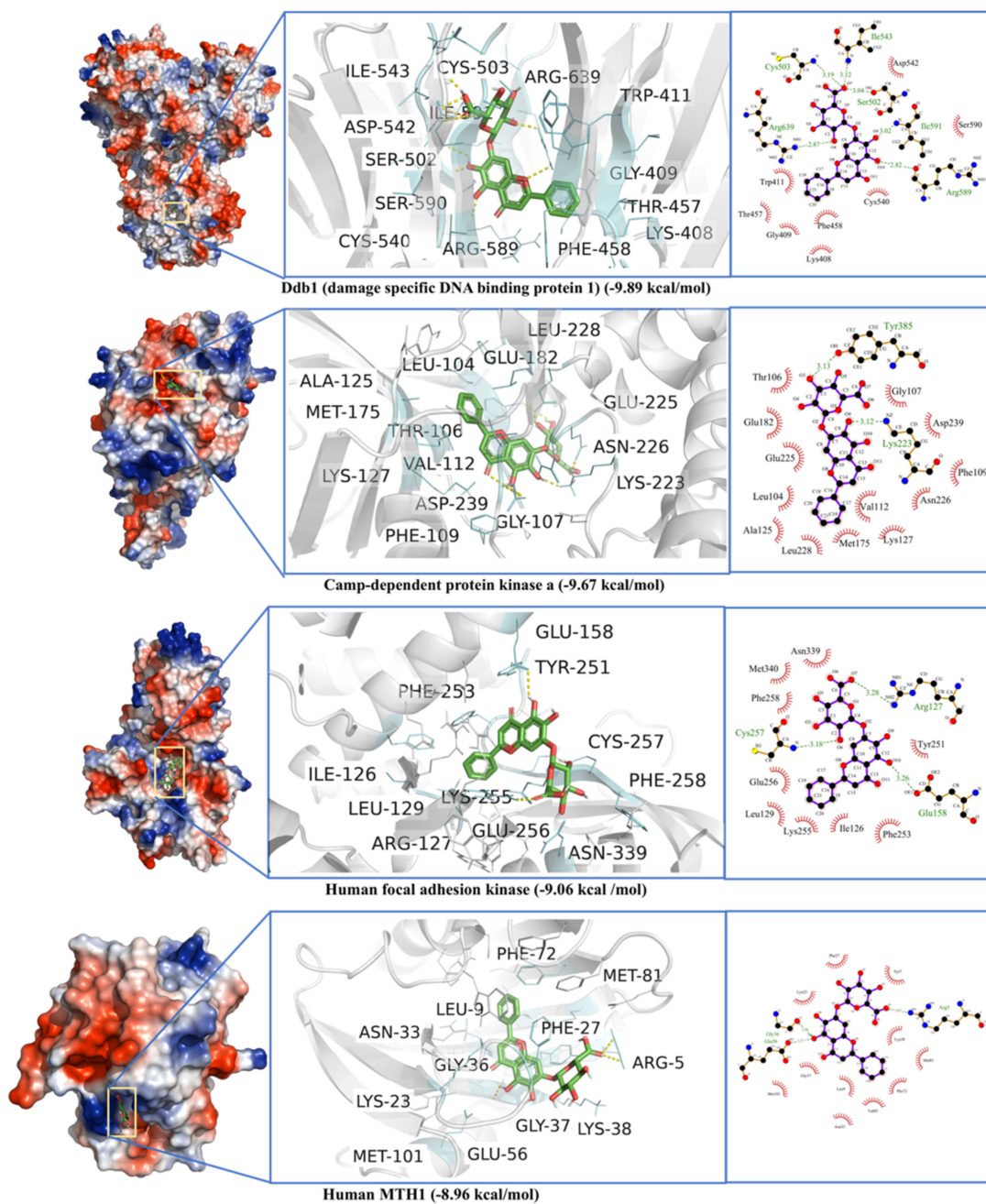
Glycyrrhizin, Hesperidin, and Baicalin were docked to a local library of selected human blood proteins (a total of 100 blood proteins) to map non-specific interactions of these ligands with non-specific proteins (Table S2). Glycyrrhizin showed the highest binding affinity against DdB1 (damage-specific DNA binding protein) with a binding energy of $-11.36 \text{ kcal}\cdot\text{mol}^{-1}$ and a dissociation constant of 1.68 nM. The interactions residues included Asn¹⁶, Gly¹⁷, Cys¹⁸, Val¹⁹, Thr²⁰, Glu⁶⁵, Leu⁶⁶, Thr¹¹⁸, Ile¹²¹, Ile¹²³, Ile¹²⁴, Asp¹²⁵, Pro¹²⁶, Asp¹⁶⁶, Lys¹⁶⁸, Phe¹⁶⁹, Tyr¹⁷¹, Ser²¹⁷, Met²¹⁸, Ala²²¹, Val²⁵⁹, Cys²⁶⁰, His²⁶¹, Asn²⁶², Arg²⁶³, Glu³¹², Cys³¹³, and Leu³¹⁴ (Figure 13a). Baicalin also interacts with DdB1 at the same binding site (Figure 13b). In non-specific interactions, Hesperidin shows the highest binding affinity (binding energy -10.89 , and dissociation constant 10.4 nM) for Integrin alpha V Beta 6 head protein normally involved in cell adhesion (Figure 13c). The

top four non-specific interacting partners of Glycyrrhizin, Hesperidin, and Baicalin are detailed in Figure 13a–c. In contrast, the binding energies and dissociations constants for all 100 non-specific proteins are given in Table S2.



(a)

Figure 13. Cont.



(b)

Figure 13. Cont.

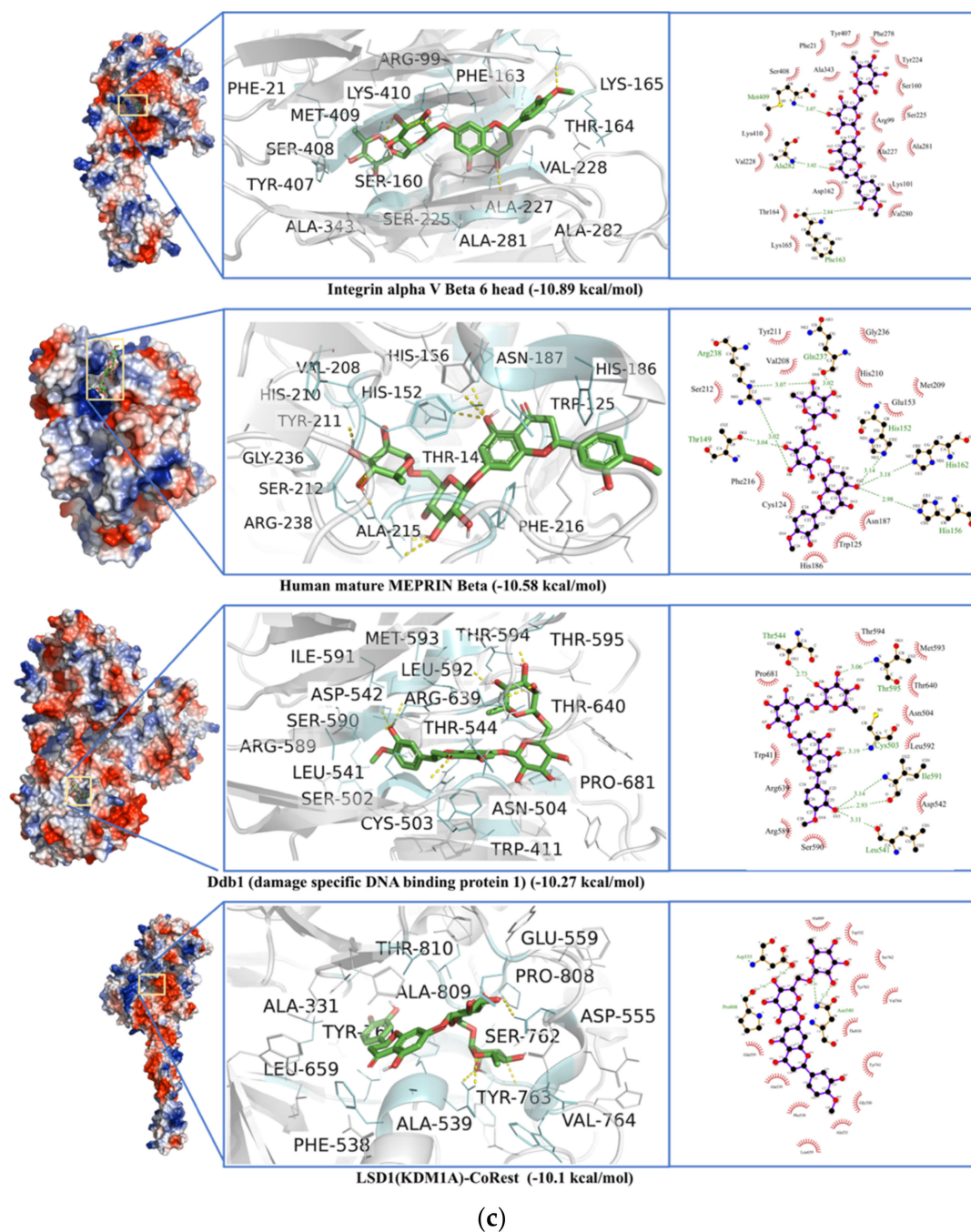


Figure 13. (a) Glycyrrhizin non-specific interactions with human proteins including Ddb1 (damage specific DNA binding protein 1), Human RECQ-like helicase, PI3KA (transferase), and Human OSC (an isomerase). (b) Baicalin non-specific interactions with damage specific DNA binding protein 1 (Ddb1), Camp-dependent protein kinase a (catalytic alpha subunit), Human focal adhesion kinase, and Human MTH1 (a hydrolase). (c) Hesperidin non-specific interactions with Integrin alpha V Beta 6 head, Human mature MEPRIN Beta (a hydrolase), Ddb1 (damage specific DNA binding protein 1), and LSD1(KDM1A)-CoRest (a transcription protein).

2.8. ADMET Properties of Selected Ligands

Lipinski's Rule of Five [46], Ghose filter (Amgen) [47], Veber's (GSK) [48] rules are used to predict ADME properties. According to the pharmacokinetic properties, all compounds show Gastrointestinal low absorption except 18- β glycyrrhetic acid (GA), lopinavir, and euchrestaflavanone A, which have high absorption. These compounds have the least BBB permeability, and no CYP inhibition was observed (Table 2).

Table 2. ADMET properties of selected ligands.

Compounds	Molecular Formula	Molecular Weight	HBA	HBD	TPSA	Log P−0.7–5	Log S 0–6	GI Absorption	BBB Permeant	CYP1A2 Inhibitor	CYP2D6 Inhibitor	Log Kp (Skin Permeation), cm/s	Lipinski Violations	Ghose Violations	Veber Violations	Bioavailability Score
Glycyrrhizin	C ₄₂ H ₆₂ O ₁₆	822.93	16	8	267.04	1.49	−6.24	Low	No	No	No	−9.33	3 MW > 500, NorO > 10, NHorOH > 5	3 MW > 480, MR > 130, atoms > 70	1 TPSA > 140	0.11
18,β Glycyrrhetic acid	C ₃₀ H ₄₆ O ₅	470.68	4	2	74.6	5.13	−6.15	High	No	No	No	−4.27	1 MLOGP4.16	3 WLOGP > 5.6, MR > 130.	Yes	1.56
Rhodiolin	C ₂₅ H ₂₀ O ₁₀	480.42	10	5	159.05	2.3	−4.99	Low	No	No	No	−7.02	0	1 MW > 480	1 TPSA > 140	0.55
Baicalin	C ₂₁ H ₁₈ O ₁₁	446.36	11	6	187.12	0.25	−3.41	Low	No	No	No	−8.23	3 NorO.10, NHorOH > 5	Yes	1 TPSA > 140	0.11
Hesperidin	C ₂₈ H ₃₄ O ₁₅	610.56	15	8	234.29	−1.06	−3.28	Low	No	No	No	−10.12	3 MW > 500, NorO > 10, NHorOH > 5	4 MW > 480, WLOGP < 0.4, MR > 130, #atoms > 70	1 TPSA > 140	0.17
Solophenol A	C ₃₀ H ₃₆ O ₆	492.6	6	4	107.22	5.69	−7.5	Low	No	No	No	−3.8	0	4 MW > 480, WLOGP < 0.4, MR > 130, #atoms > 71	1 TPSA > 140	0.55
Naringin	C ₂₆ H ₃₀ O ₁₄	566.51	14	8	225.06	−0.99	−2.68	Low	No	No	No	−10.39	3 MW > 500, NorO > 10, NHorOH > 5	3MW > 480, WLOGP < 0.4 MR > 130,	1 TPSA > 140	0.17
Lopinavir	C ₃₇ H ₄₈ N ₄ O ₅	628.8	5	4	120	4.37	−6.64	High	No	No	No	−5.93	1 MW > 500	3 MW > 480, MR > 130, #atoms > 70	1 Rotors > 10	0.55

HBA: Number of Hydrogen bond acceptors HBD: Number of hydrogen bond donor, TPSA: Topological polar surface area.

3. Discussion

Antioxidants including Glycyrrhizin, 18, β Glycyrrhetic acid, Rhodiolin, Baicalin, and Hesperidin have shown remarkable potential in targeting various SARS-CoV-2 enzymes and proteins. Glycyrrhizin, largely found in licorice root, has already been found active against many viral proteases, including herpesviruses [49,50], flaviviruses [51], and Human Immunodeficiency Virus [52]. Glycyrrhizin was already used to treat patients with hepatitis C [53] and upper respiratory tract infections [54]. Glycyrrhizin, Glycyrrhizic acid, its other derivatives and Baicalin were the first compounds found active against SARS coronavirus (SARS-CoV-1) [55,56]. Flavonoids and their derivatives have been reported to inhibit various SARS-CoV-2 proteins [57]. Hesperidin and quercetin have also been found good antiviral agents [58,59].

The binding site for M^{Pro} has already been defined by X-ray crystallographic structure (PDB ID 6WQF) obtained at room temperature [38] where His⁴¹ and Cys⁴⁵ form a catalytic dyad to interact with bound ligand. Other amino acids involved in the stabilization of the active site were Ser⁴⁶, Leu¹⁴¹, Asn¹⁴², Glu¹⁶⁶, Pro¹⁶⁸, Gln¹⁸⁹, Thr¹⁹⁰, Ala¹⁹¹. This active site is situated in a cleft between domains I and II [60,61]. In our study, Glycyrrhizin shows two binding sites; one includes the conventional active site of the enzyme, while the second interactions include an allosteric binding site. A previous docking analysis of Glycyrrhizin against M^{Pro} has shown a binding energy value $-7.81 \text{ kcal}\cdot\text{mol}^{-1}$ where it interacts with the proposed active site of the enzyme [62]. In another study, glycyrrhizic acid, Glabridin and Liquiritigenin show strong binding interactions (with a binding energy of -7.0 to $-8.0 \text{ kcal}\cdot\text{mol}^{-1}$) with M^{Pro} conventional active site [63]. The docking analysis of M^{Pro} with FDA-approved anti-viral compounds and library of active phytochemicals [64] shows Nelfinavir potent against M^{Pro}. Many natural compounds are found to be potential inhibitors of M^{Pro}, including Leucofedin [65], Leupeptin [66], Rutin [67], cannabisin-A, isoacetoside [68], epigallocatechin gallate, and epicatechin gallate [69]. Recently, Glycyrrhizin has been found to indirectly inhibit the SARS-CoV-2 replication by inhibiting M^{Pro} enzyme activity [70]. In our study, many ligands, including Glycyrrhizin, have been found to interact with M^{Pro} allosteric binding sites (Table 1 and Table S1, Figure 2). In a previous study, 2400 FDA-approved drugs have been screened against M^{Pro} allosteric binding sites, where selinexor, bromocriptine, Dihydroergotamine, nilotinib, entrectinib, digitoxin, and diosmin have shown promising binding to the enzyme [71].

PL^{Pro} consists of an N-terminal ubiquitin-like (Ubl) domain (1–60 a.a) and a catalytic region with a right-handed thumb-palm-fingers architecture. The PL^{Pro} binding site is found in the thumb and palm domain and is characterized by the presence of a catalytic triad (Cys¹¹¹, His²⁷², and Asp²⁸⁶) [72]. In our study, Baicalin and Hesperidin have been found to be potential PL^{Pro} inhibitors that interact with their proposed active site (Figure 4). GRL0617 with PL^{Pro} shows binding to the same site [73], whereas π - π interactions with Tyr²⁶⁸ have shown definite inhibition of PL^{Pro} activity. Natural compounds like Caesalpininaphenol A, and Sappanone B, also interact with Tyr²⁶⁸. Corylifol A, chromen, darunavir, sofosbuvir and some other drugs were screened against PL^{Pro}. These drugs were found to bind near the proposed catalytic triad [74]. Phytochemicals from *Vitex negundo* L. are also found active against PL^{Pro} [75]. Along with natural compounds, many approved antibacterial and antiviral drugs also have been repurposed [76–78].

Here, MD simulations validate the role of Tyr²⁶⁸ in Baicalin, Hesperidin, and Solophenol enzyme complexes (Figure 5). All catalytic residues seem to interact with these ligands in 30 ns MD simulation. In a previous study, MD simulations for PL^{Pro} were found stabilized after 12 ns and remained stable until 50 ns [79]. Baicalin can be extracted from the roots of *Scutellaria baicalensis* Georgi. In another study, six phytochemicals, including Baicalin, rutin, biopterin, licoleafol, luteolin, and quercetin, have shown binding to PL^{Pro} [80]. In addition, Baicalin showed antiviral activity against dengue virus (DENV) [81], Influenza A virus (IAV) [82], Zika virus (ZIKV) [83], Chikungunya virus (CHIKV) [84], and Human Immunodeficiency Virus 1 (HIV-1) [85].

Glycyrrhizin, Hesperidin, and Biacalin show strong interactions with RdRp. Glycyrrhizin binds in the enzyme's potential active site pocket while making H-bonding with Asp⁷⁶⁰ and other residues (Figure 6). Asp^{760,761} have been proposed as active site residues, while Tyr⁶¹⁹, Cys⁶²², Ser⁷⁵⁹, Ala⁷⁶², Glu⁸¹¹, Cys⁸¹³, and Ser⁸¹⁴ are found in potential binding sites for Ribavirin, Remdesivir, and other antiviral interactions [86]. In a screening with flavonoid compounds, Delphinidin 3-O-beta-D-glucoside 5-O-(6-coumaroyl-beta-D-glucoside) complex with RdRp has been found most stable, where Asp^{760,761} have been found in the ligand-binding site [87]. Lanreotide, Argiprestocin, Demoxytocin, and Polymyxin B1 also interact with Asp⁷⁶⁰. Previously, polyphenols with binding energy <7.0 have been reported to interact with RdRp, while Remdesivir showed binding energy of 7.9 kcal·mol⁻¹ [88] and interacts with a similar ligand-binding site as for Glycyrrhizin, Hesperidin. This site includes Asp^{760,761}, and Glu⁸¹¹ for Remdesivir [89,90]. In another study, approved antivirals including Ribavirin, Remdesivir, Sofosbuvir, Galidesivir, and Tenofovir have shown strong interactions with RdRp, where Ribavirin have shown binding energy of -8.7 kcal/mol [86]. Many compounds from the ZINC database have been screened against RdRp and 40 ns MD simulations were performed for Rifabutin, ZINC09128258 and ZINC09883305 [91].

Glycyrrhizin strongly binds to the S2 subunit of the spike protein. Although the binding residues are different from the receptor-binding domain (331–524 a.a.), it is expected that this interaction may bring the conformation change in the protein that may affect the receptor binding. This conformational change is also indicated by MD simulation showing large RMSD and RMSF changes in the receptor-binding region and formation of the close complex (low R_g) (Figure 8 and Figure S4). A number of flavonoid compounds were docked to spike protein and naringin has been found as the most potent compound against SARS-CoV-2 spike protein [92]. In our study, Glycyrrhizin showed the best binding energy against the open and close state of spike glycoproteins. Most of the Glycyrrhizin's interactions have been found with the S2 subunit of the spike protein (Figure 8b). In one study, 66 compounds were found to interact with RBD of spike protein and Glycyrrhizic acid was found to be the most potent antiviral and spike protein inhibitor [93]. Rhodiolin and Hesperidin bind to the N-terminal domain of spike protein and show the second-best binding energies (Figure 8b). Mutations in spike protein lead to new SARS-CoV-2 variants. Glycyrrhizin was docked against the spike protein variants initially reported from Brazil (B.1.1.28), South Africa (B.1.351), and the United Kingdom (B.1.1.17). The variant B.1.1.7 was first reported in the United Kingdom on 14 December 2020 [94,95], B.1.1.28 originated from Brazil [96]. Both mutations, B.1.1.7 and B.1.1.28, carry the N501Y mutation in the RBD of the spike protein. Later, the B.1.351 variant (20H/501Y.V2) was first reported in South Africa [97], was marked by mutation of K417N and E484K in the RBD region of the spike protein. Surprisingly, the affinity of the Glycyrrhizin slightly decreased against the spike protein variants, though it still shows considerable binding energy and dissociation constant (Figure S6). Catechins and tamibarotene have been found to interact strongly with the UK variant and triple SARS-CoV-2 variant [98,99].

In the case of SARS-CoV-2 helicase, the interface between RecA1 and RecA2 domains contains the active site residues for helicase enzyme, including Lys²⁸⁸, Ser²⁸⁹, Asp³⁷⁴, Glu³⁷⁵, Gln⁴⁰⁴, and Arg⁵⁶⁷ [100,101]. In this study, Glycyrrhizin binds to an allosteric site near the catalytic cleft, while Glycyrrhetic acid interacts with residues in stalk and 1B domain. Triphenylamine and Darunavir have been reported to bind the same active site [102]. Rutin, xanthenes, and many other polyphenols have been reported to be ATPase inhibitors [59]. A database of 14,000 phytochemicals has been docked against helicase using virtual screening; out of them, 368 compounds have been found to be potent helicase inhibitors [103]. Picrasidine M from a herb *Picrasma quassioides* shows the best binding to helicase, where it forms 2 H-bonds with Ser²⁸⁹ and one H-bond with Gln⁴⁰⁴ and Arg⁵⁶⁷ [103]. E-channel blockers are demonstrated to be potent antivirals by protecting hosts cells from death. Glycyrrhizin, Glycyrrhetic acid, and Baicalin have also shown

binding to E-channel protein. Proanthocyanidins have been reported to inhibit the MPro and E-channel protein of the SARS-CoV-2 [104].

Glycyrrhizin seems to interact with four SARS-CoV-2 key proteins with high affinity, where its binding with helicase and RdRp has been found to be more stable (Figure 14). Glycyrrhizin has also been reported to interact with TMPRSS2, involved in viral penetration into the host cells [105]. It also indicates that licorice root, a potential source of Glycyrrhizin, may be used as a possible cure and a household remedy for COVID-19. The non-specific interactions of Glycyrrhizin show that it may interact with Ddb1 and other non-specific human blood proteins. Glycyrrhizin as Glycyrrhizic acid from *Glycyrrhiza glabra* and as a derivative in the form of β -Glycyrrhetic acid are reported to show penetration through the blood-brain barrier and are non-carcinogenic [63] (Table 2). This study shows that natural antioxidant compounds, either partially purified or in crude form, may provide protection against SARS-CoV-2 severity and complications by interacting with its key enzymes. Although we have performed 30 ns MD simulations as in the case of many protein-ligand complexes equilibrium was achieved and complex was found stable, longer MD simulations (>100 ns) in future studies may help to better understand the behavior and stability of the complexes. In vivo studies for the selected compounds are also recommended to probe the computational result and may help in the formulation of natural antivirals with less toxicity and more efficacy.

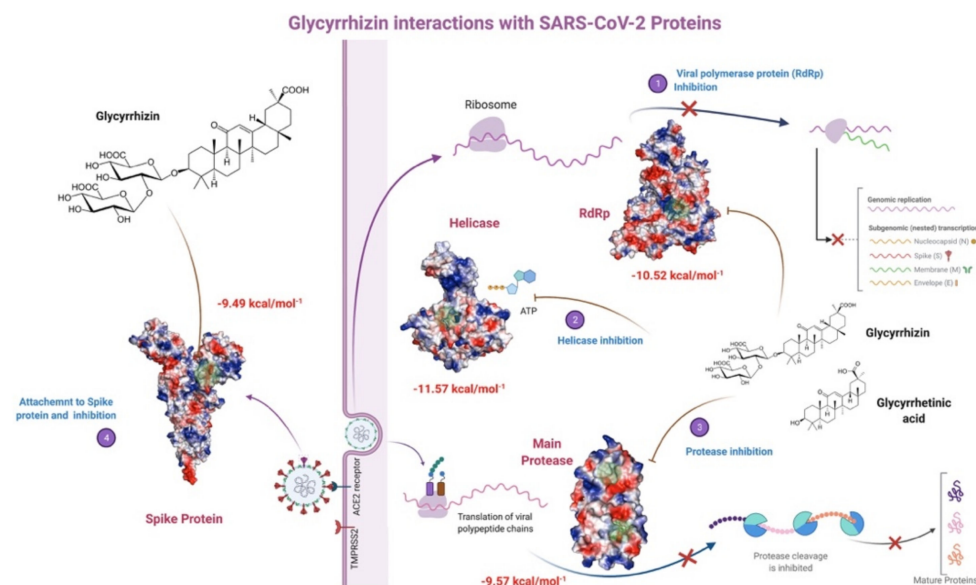


Figure 14. Glycyrrhizin interactions with SARS-CoV-2 proteins (prepared with bio renderer).

4. Conclusions

In the current pandemic situation, COVID-19's battle with humanity is still continued. The availability of various vaccines has eased the aggravating situation, but the rise of SARS-CoV2 variants warns that humans have to live with the virus, evading its devastating effects. Potential natural cures/medications/home remedies without any side effects seems a viable solution in the current circumstances. Our study has examined and screened more than a hundred natural compounds from plants against six SARS CoV-2 proteins by using molecular docking and molecular dynamics simulations to identify potential bioactive compounds. Glycyrrhizin was found as the best ligand showing strong inhibition of five SARS CoV-2 proteins. Glycyrrhizin is present in a large amount in an inexpensive household herb licorice already registered for its magical curative properties against a number of diseases. Other phytochemicals found potent against SARS-CoV2 include Hesperidin and Baicalin present in citrus fruits and many other plants. In our study, Glycyrrhizin, Hesperidin, and Baicalin were docked against non-specific human blood proteins and have shown interactions with DNA binding proteins. Based on our findings,

we suggest that further in vivo evaluation of Glycyrrhizin and its sister compounds as potential antivirals will signify their role in the treatment and management of COVID-19.

5. Materials and Methods

A total of 115 natural compounds with established therapeutic properties were targeted against six SARS-CoV-2 proteins by molecular docking. The compound structures were obtained from various chemical databases, including PubChem (<https://pubchem.ncbi.nlm.nih.gov/>, accessed on 25 March 2021), ChemSpider (<https://chemspider.com>, accessed on 25 March 2021) and MolPort (<https://www.molport.com/>, accessed on 25 March 2021) (Table S1). The compound structures were obtained in form of The Spatial Data File (SDF) and optimized using the MM1 forcefield in YASARA Structure ver. 20.7.4 [106]. The ligand structures were merged in a single file prepared for virtual screening. Six SARS-CoV-2 proteins were obtained from Protein Data Bank (PDB), including Main Protease (M^{Pro}, PDB ID 6Y84), Papain-like protease (PL^{Pro}, PDB ID 6WX4), RNA-dependent RNA polymerase (RdRp, PDB ID 6M71), Spike Glycoprotein (S, open and closed state, PDB IDs 6VXX and 6VYB), Helicase (Nsp13) (PDB ID 6ZSL), and E-Channel (Envelop small membrane protein) (PDB ID 5 × 29) (Figure 1). Spike protein variants' structures as well as structures for all selected non-specific proteins were also obtained from PDB (Table S2a–c). The single-chain structures for all proteins were prepared using YASARA Structure ver. 20.7.4 [106] and heteroatoms were removed.

5.1. Molecular Docking

The ligand-protein interactions and binding energies were calculated by applying a virtual screening module in YASARA software version 20.7.4 [106] that uses a modified AutoDock-Lamarckian Genetic Algorithm. The parameters used for the virtual screening and molecular docking have been described earlier [107], where AMBER03-FF was used with a hundred global docking runs and by keeping the random seed value of 1000. AutoDock local search (LGA-LS) was also used for selected top five ligands to reassure best binding and energy minimization. Protein-ligand interactions were mapped in terms of binding energies and dissociation constants, while the docking scores were calculated by Equation (1)

$$\Delta G = \Delta G_{(\text{van der Waals})} + \Delta G_{(\text{H-bonding})} + \Delta G_{(\text{electrostatic})} + \Delta G_{(\text{torsional free energy})} + \Delta G_{(\text{desolvation energy})} \quad (1)$$

LigPlus [108] was used to obtain and ligand-protein interactions. The specific ligand was selected in the ligand-protein complex file and interactions including H-bonds were mapped. Non-specific Interactions of selected ligands against human blood proteins were studied by an inverse docking procedure where more than 100 human blood protein targets were screened against the selected ligands (Table S2a–c).

5.2. Molecular Dynamic Simulations

Molecular Dynamic simulations (MDS) were performed using YASARA Structure ver. 20.7.4 [106] with AMBER14 as a force field as described before [109]. The simulation cell was prepared by providing 20 Å water-filled space around the fully mobile protein with a density of 0.997 g/mL. The system was neutralized with 0.9% NaCl while maintaining 298 K temperature, pH 7.4, periodic boundaries, and 7.86 cut-off for long-range coulomb electrostatics forces. After the initial steepest descent minimization, MDS was performed at the rate of 1.25–2.50 fs time steps, and the simulation snapshot was saved every 100 ps. MDS of 10–30 ns were calculated for different proteins depending on the number of atoms in the simulation cell. The raw data were analyzed using GraphPad Prism ver. 7.0. [110]. RMSD and RMSF values were tabulated and analyzed for the fluctuations. A docking and MD simulation flow chart had been given in Figure 15.

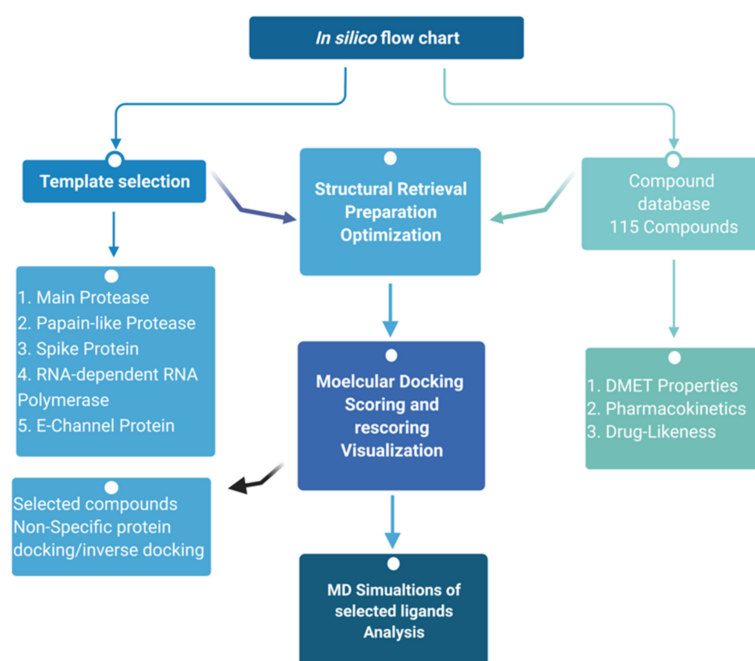


Figure 15. Flow diagram of Methodology.

5.3. Pharmacokinetics and Drug-Likeness

The pharmacokinetic properties and drug-likeness prediction of the top 10 li were performed by the SwissADME server (<http://www.swissadme.ch/>, accessed on 20 April 2021). It calculates the topological polar surface area (TPSA), logP (lipophilicity), and logS (solubility). The drug-likeness was predicted by following Lipinski, Ghose, and Veber rules and bioavailability scores [46–48]. The Lipinski’s Rule of Five states that the absorption or permeation of a molecule is more likely when the molecular mass is under 500 g/mol, the value of log P is lower than 5, and the molecule has utmost 5 H-donor and 10 H-acceptor atoms [46]. Ghose filter (Amgen) [47] defines drug-likeness based on log P between -0.4 – 5.6 , MW between 160–480, molar refractivity between 40–130, and the total number of atoms between 20–70. Veber (GSK) [48], the rule defines drug-likeness as rotatable bond count ≤ 10 and polar surface area (PSA) ≤ 140 .

Supplementary Materials: The following are available online at <https://www.mdpi.com/article/10.3390/antibiotics10081011/s1>, Figure S1: 30 ns Molecular dynamics simulation of Glycyrrhizin (blue) and Rhodiolin (red) docked with SARS-CoV-2 main protease (MPro), Figure S2: 30 ns Molecular dynamics simulation of Baicalin (red), Hesperidin (green), and Solophenol (blue) docked with SARS-CoV-2 PLpro, Figure S3: 30 ns Molecular dynamics simulation of Glycyrrhizin (red), Hesperidin (green), Baicalin (blue) in complex with SARS-CoV-2 RdRp. Figure S4: 30 ns Molecular dynamics simulation of Glycyrrhizin (red) and Hesperidin (green) in complex with SARS-CoV-2 spike protein (closed state) Figure S5: 30 ns Molecular dynamics simulation of Glycyrrhizin (red), Hesperidin (green), Baicalin (blue) in complex with SARS-CoV-2 helicase Figure S6: Glycyrrhizin interactions with variants of Spike protein of SARS-CoV-2, Table S1: Ligands docked to the SARS-CoV-2 proteins; binding energies, dissociation constants and active sites, Table S2a: Glycyrrhizin docking to nonspecific human blood proteins, Table S2b: Baicalin docking to nonspecific human blood proteins, Table S2c: Hesperidine docking to nonspecific human blood proteins and Table S3.

Author Contributions: Conceptualization, M.F.u.R. and M.A.; methodology, M.F.u.R., A.I.B. and S.A.; software, M.F.u.R., R.E. and S.A.; validation, M.F.u.R., M.S.A., M.S. and F.K.; formal analysis, S.A. and R.E.; investigation, S.A., R.E. and A.I.B.; resources, M.F.u.R., M.S.A. and C.L.; data curation, S.A. and M.S.; writing—original draft preparation, S.A., M.F.u.R., M.S.; writing—review and editing, M.F.u.R., S.A., C.L. and M.S.A.; visualization, C.L., Z.S. and M.F.u.R.; supervision, M.F.u.R.; project administration, M.F.u.R., M.S., C.L., Z.S. and M.M.; funding acquisition, M.F.u.R., M.M. and C.L. All authors have read and agreed to the published version of the manuscript.

Funding: Funding in the C.L. lab was provided by the Fundamental Research Funds for the Central Universities (2232021G-04), Shanghai Science and Technology Committee (19ZR1471100). M.F.u.R. is thankful to the Office and Research and Innovation Centre (ORIC), University of Sargodha, Sargodha, Pakistan, for the award of COVID-19 related research Project awarded via number SU/ORIC/923. M.F.u.R. is also thankful for online utilization of computational resources at C.L. lab, Donghua University, China.

Conflicts of Interest: The authors declare no conflict of interest.

References

1. Yang, Y.; Peng, F.; Wang, R.; Guan, K.; Jiang, T.; Xu, G.; Sun, J.; Chang, C. The deadly coronaviruses: The 2003 SARS pandemic and the 2020 novel coronavirus epidemic in China. *J. Autoimmun.* **2020**, *109*, 102434. [CrossRef]
2. Rehman, M.F.; Fariha, C.; Anwar, A.; Shahzad, N.; Ahmad, M.; Mukhtar, S.; Haque, M.F.U. Novel coronavirus disease (COVID-19) pandemic: A recent mini review. *Comput. Struct. Biotechnol. J.* **2020**, *19*, 612–623. [CrossRef]
3. Coronavirus-Worldwide-Graphs. Available online: <https://www.worldometers.info> (accessed on 12 August 2021).
4. Dinleyici, E.C.; Borrow, R.; Safadi, M.A.P.; Van Damme, P.; Munoz, F.M. Vaccines and routine immunization strategies during the COVID-19 pandemic. *Hum. Vaccines Immunother.* **2021**, *17*, 400–407. [CrossRef]
5. Mazzola, A.; Todesco, E.; Drouin, S.; Hazan, F.; Marot, S.; Thabut, D.; Varnous, S.; Soulié, C.; Barrou, B.; Marcelin, A.-G.; et al. Poor Antibody Response After Two Doses of Severe Acute Respiratory Syndrome Coronavirus 2 (SARS-CoV-2) Vaccine in Transplant Recipients. *Clin. Infect. Dis.* **2021**. [CrossRef]
6. Mohammed, F.S.; Akgul, H.; Sevindik, M.; Khaled, B.M.T. Phenolic content and biological activities of *Rhus coriaria* var. *zebaria*. *Fresenius Environ. Bull.* **2018**, *27*, 5694–5702.
7. Sevindik, M.; Akgul, H.; Selamoglu, Z.; Braidy, N. Antioxidant and antigenotoxic potential of *infundibulicybe geotropa* mushroom collected from Northwestern Turkey. *Oxidative Med. Cell. Longev.* **2020**, *2020*, 5620484. [CrossRef] [PubMed]
8. Sevindik, M.; Akgul, H.; Bal, C.; Selamoglu, Z. Phenolic contents, oxidant/antioxidant potential and heavy metal levels in *Cyclocybe cylindracea*. *Indian J. Pharm. Educ. Res.* **2018**, *52*, 437–441. [CrossRef]
9. Mani, J.S.; Johnson, J.B.; Steel, J.C.; Broszczak, D.A.; Neilsen, P.M.; Walsh, K.B.; Naiker, M. Natural product-derived phytochemicals as potential agents against coronaviruses: A review. *Virus Res.* **2020**, *284*, 197989. [CrossRef]
10. Li, S.-y.; Chen, C.; Zhang, H.-q.; Guo, H.-y.; Wang, H.; Wang, L.; Zhang, X.; Hua, S.-n.; Yu, J.; Xiao, P.-g. Identification of natural compounds with antiviral activities against SARS-associated coronavirus. *Antivir. Res.* **2005**, *67*, 18–23. [CrossRef]
11. Kim, J.Y.; Kim, Y.I.; Park, S.J.; Kim, I.K.; Choi, Y.K.; Kim, S.-H. Safe, high-throughput screening of natural compounds of MERS-CoV entry inhibitors using a pseudovirus expressing MERS-CoV spike protein. *Int. J. Antimicrob. Agents* **2018**, *52*, 730. [CrossRef] [PubMed]
12. Yang, X.; Yu, Y.; Xu, J.; Shu, H.; Liu, H.; Wu, Y.; Zhang, L.; Yu, Z.; Fang, M.; Yu, T. Clinical course and outcomes of critically ill patients with SARS-CoV-2 pneumonia in Wuhan, China: A single-centered, retrospective, observational study. *Lancet Respir. Med.* **2020**, *8*, 475–481. [CrossRef]
13. Huang, C.; Wang, Y.; Li, X.; Ren, L.; Zhao, J.; Hu, Y.; Zhang, L.; Fan, G.; Xu, J.; Gu, X. Clinical features of patients infected with 2019 novel coronavirus in Wuhan, China. *Lancet* **2020**, *395*, 497–506. [CrossRef]
14. Mao, R.; Qiu, Y.; He, J.-S.; Tan, J.-Y.; Li, X.-H.; Liang, J.; Shen, J.; Zhu, L.-R.; Chen, Y.; Iacucci, M. Manifestations and prognosis of gastrointestinal and liver involvement in patients with COVID-19: A systematic review and meta-analysis. *Lancet Gastroenterol. Hepatol.* **2020**, *5*, 667–678. [CrossRef]
15. Van Norman, G.A. Drugs, Devices, and the FDA: Part 1: An Overview of Approval Processes for Drugs. *JACC: Basic Transl. Sci.* **2016**, *1*, 170–179. [CrossRef]
16. Li, G.; De Clercq, E. *Therapeutic Options for the 2019 Novel Coronavirus (2019-nCoV)*; Nature Publishing Group: Berlin, Germany, 2020.
17. Savarino, A.; Di Trani, L.; Donatelli, I.; Cauda, R.; Cassone, A. New insights into the antiviral effects of chloroquine. *Lancet Infect. Dis.* **2006**, *6*, 67–69. [CrossRef]
18. Yan, Y.; Zou, Z.; Sun, Y.; Li, X.; Xu, K.-F.; Wei, Y.; Jin, N.; Jiang, C. Anti-malaria drug chloroquine is highly effective in treating avian influenza A H5N1 virus infection in an animal model. *Cell Res.* **2013**, *23*, 300–302. [CrossRef]
19. Savarino, A.; Boelaert, J.R.; Cassone, A.; Majori, G.; Cauda, R. Effects of chloroquine on viral infections: An old drug against today's diseases. *Lancet Infect. Dis.* **2003**, *3*, 722–727. [CrossRef]
20. Mizui, T.; Yamashina, S.; Tanida, I.; Takei, Y.; Ueno, T.; Sakamoto, N.; Ikejima, K.; Kitamura, T.; Enomoto, N.; Sakai, T. Inhibition of hepatitis C virus replication by chloroquine targeting virus-associated autophagy. *J. Gastroenterol.* **2010**, *45*, 195–203. [CrossRef]
21. Farias, K.J.S.; Machado, P.R.L.; De Almeida Junior, R.F.; De Aquino, A.A.; Da Fonseca, B.A.L. Chloroquine interferes with dengue-2 virus replication in U937 cells. *Microbiol. Immunol.* **2014**, *58*, 318–326. [CrossRef]
22. Delvecchio, R.; Higa, L.M.; Pezzuto, P.; Valadão, A.L.; Garcez, P.P.; Monteiro, F.L.; Loiola, E.C.; Dias, A.A.; Silva, F.J.; Aliota, M.T. Chloroquine, an endocytosis blocking agent, inhibits Zika virus infection in different cell models. *Viruses* **2016**, *8*, 322. [CrossRef]
23. Dowall, S.D.; Bosworth, A.; Watson, R.; Bewley, K.; Taylor, I.; Rayner, E.; Hunter, L.; Pearson, G.; Easterbrook, L.; Pitman, J. Chloroquine inhibited Ebola virus replication in vitro but failed to protect against infection and disease in the in vivo guinea pig model. *J. Gen. Virol.* **2015**, *96*, 3484. [CrossRef]

24. Vincent, M.J.; Bergeron, E.; Benjannet, S.; Erickson, B.R.; Rollin, P.E.; Ksiazek, T.G.; Seidah, N.G.; Nichol, S.T. Chloroquine is a potent inhibitor of SARS coronavirus infection and spread. *Virology* **2005**, *2*, 69. [\[CrossRef\]](#)
25. Fiolet, T.; Guihur, A.; Rebeaud, M.; Mulot, M.; Peiffer-Smadja, N.; Mahamat-Saleh, Y. Effect of hydroxychloroquine with or without azithromycin on the mortality of COVID-19 patients: A systematic review and meta-analysis. *Clin. Microbiol. Infect.* **2020**, *27*, 19–27. [\[CrossRef\]](#) [\[PubMed\]](#)
26. Roustit, M.; Guilhaumou, R.; Molimard, M.; Drici, M.D.; Laporte, S.; Montastruc, J.L. Chloroquine and hydroxychloroquine in the management of COVID-19: Much kerfuffle but little evidence. *Therapies* **2020**, *75*, 363–370. [\[CrossRef\]](#) [\[PubMed\]](#)
27. Tang, W.; Cao, Z.; Han, M.; Wang, Z.; Chen, J.; Sun, W.; Wu, Y.; Xiao, W.; Liu, S.; Chen, E.; et al. Hydroxychloroquine in patients mainly with mild to moderate COVID-19: An open-label, randomized, controlled trial. *medRxiv* **2020**. [\[CrossRef\]](#)
28. Borba, M.; De Almeida Val, F.; Sampaio, V.S.; Alexandre, M.A.; Melo, G.C.; Brito, M.; Mourao, M.; Sousa, J.D.B.; Guerra, M.V.F.; Hajjar, L.; et al. Chloroquine diphosphate in two different dosages as adjunctive therapy of hospitalized patients with severe respiratory syndrome in the context of coronavirus (SARS-CoV-2) infection: Preliminary safety results of a randomized, double-blinded, phase IIb clinical trial (CloroCovid-19 Study). *medRxiv* **2020**. [\[CrossRef\]](#)
29. Guaraldi, G.; Meschiari, M.; Cozzi-Lepri, A.; Milic, J.; Tonelli, R.; Menozzi, M.; Franceschini, E.; Cuomo, G.; Orlando, G.; Borghi, V.; et al. Tocilizumab in patients with severe COVID-19: A retrospective cohort study. *Lancet Rheumatol.* **2020**, *2*, e474–e484. [\[CrossRef\]](#)
30. Cortegiani, A.; Ippolito, M.; Greco, M.; Granone, V.; Protti, A.; Gregoretti, C.; Giarratano, A.; Einav, S.; Cecconi, M. Rationale and evidence on the use of tocilizumab in COVID-19: A systematic review. *Pulmonology* **2020**, *27*, 52–66. [\[CrossRef\]](#) [\[PubMed\]](#)
31. Della-Torre, E.; Campochiaro, C.; Cavalli, G.; De Luca, G.; Napolitano, A.; La Marca, S.; Boffini, N.; Da Prat, V.; Di Terlizzi, G.; Lanzillotta, M.; et al. Interleukin-6 blockade with sarilumab in severe COVID-19 pneumonia with systemic hyperinflammation: An open-label cohort study. *Ann. Rheum. Dis.* **2020**, *79*, 1277–1285. [\[CrossRef\]](#)
32. Chen, L.; Xiong, J.; Bao, L.; Shi, Y. Convalescent plasma as a potential therapy for COVID-19. *Lancet Infect. Dis.* **2020**, *20*, 398–400. [\[CrossRef\]](#)
33. Bloch, E.M.; Shoham, S.; Casadevall, A.; Sachais, B.S.; Shaz, B.; Winters, J.L.; Van Buskirk, C.; Grossman, B.J.; Joyner, M.; Henderson, J.P. Deployment of convalescent plasma for the prevention and treatment of COVID-19. *J. Clin. Investig.* **2020**, *130*, 2757–2765. [\[CrossRef\]](#)
34. Hoffmann, M.; Schroeder, S.; Kleine-Weber, H.; Müller, M.A.; Drosten, C.; Pöhlmann, S. Nafamostat Mesylate Blocks Activation of SARS-CoV-2: New Treatment Option for COVID-19. *Antimicrob. Agents Chemother.* **2020**, *64*, e00754–20. [\[CrossRef\]](#)
35. Shalhoub, S. Interferon beta-1b for COVID-19. *Lancet* **2020**, *395*, 1670–1671. [\[CrossRef\]](#)
36. Group, T.R.C. Dexamethasone in Hospitalized Patients with Covid-19—Preliminary Report. *N. Engl. J. Med.* **2020**. [\[CrossRef\]](#)
37. Beigel, J.H.; Tomashek, K.M.; Dodd, L.E.; Mehta, A.K.; Zingman, B.S.; Kalil, A.C.; Hohmann, E.; Chu, H.Y.; Luetkemeyer, A.; Kline, S. Remdesivir for the treatment of Covid-19—Preliminary report. *N. Engl. J. Med.* **2020**, *383*, 1813–1836. [\[CrossRef\]](#)
38. Kneller, D.W.; Phillips, G.; O'Neill, H.M.; Jedrzejczak, R.; Stols, L.; Langan, P.; Joachimiak, A.; Coates, L.; Kovalevsky, A. Structural plasticity of SARS-CoV-2 3CL M(pro) active site cavity revealed by room temperature X-ray crystallography. *Nat. Commun.* **2020**, *11*, 3202. [\[CrossRef\]](#) [\[PubMed\]](#)
39. Jin, Z.; Du, X.; Xu, Y.; Deng, Y.; Liu, M.; Zhao, Y.; Zhang, B.; Li, X.; Zhang, L.; Peng, C.; et al. Structure of Mpro from SARS-CoV-2 and discovery of its inhibitors. *Nature* **2020**, *582*, 289–293. [\[CrossRef\]](#)
40. Sztain, T.; Amaro, R.; McCammon, J.A. Elucidation of Cryptic and Allosteric Pockets within the SARS-CoV-2 Main Protease. *J. Chem. Inf. Modeling* **2021**, *61*, 3495–3501. [\[CrossRef\]](#)
41. Dubanevics, I.; McLeish, T.C. Computational analysis of dynamic allostery and control in the SARS-CoV-2 main protease. *J. R. Soc. Interface* **2021**, *18*, 20200591. [\[CrossRef\]](#)
42. Goyal, B.; Goyal, D. Targeting the Dimerization of the Main Protease of Coronaviruses: A Potential Broad-Spectrum Therapeutic Strategy. *ACS Comb. Sci.* **2020**, *22*, 297–305. [\[CrossRef\]](#)
43. Osipiuk, J.; Azizi, S.-A.; Dvorkin, S.; Endres, M.; Jedrzejczak, R.; Jones, K.A.; Kang, S.; Kathayat, R.S.; Kim, Y.; Lisnyak, V.G.; et al. Structure of papain-like protease from SARS-CoV-2 and its complexes with non-covalent inhibitors. *Nat. Commun.* **2021**, *12*, 743. [\[CrossRef\]](#)
44. Rut, W.; Lv, Z.; Zmudzinski, M.; Patchett, S.; Nayak, D.; Snipas, S.J.; El Oualid, F.; Bekes, M.; Huang, T.T.; Drag, M. Activity profiling and structures of inhibitor-bound SARS-CoV-2-PLpro protease provides a framework for anti-COVID-19 drug design. *bioRxiv* **2020**. [\[CrossRef\]](#)
45. Gao, Y.; Yan, L.; Huang, Y.; Liu, F.; Zhao, Y.; Cao, L.; Wang, T.; Sun, Q.; Ming, Z.; Zhang, L.; et al. Structure of the RNA-dependent RNA polymerase from COVID-19 virus. *Science* **2020**, *368*, 779–782. [\[CrossRef\]](#)
46. Lipinski, C.A.; Lombardo, F.; Dominy, B.W.; Feeney, P.J. Experimental and computational approaches to estimate solubility and permeability in drug discovery and development settings. *Adv. Drug Deliv. Rev.* **2001**, *46*, 3–26. [\[CrossRef\]](#)
47. Ghose, A.K.; Viswanadhan, V.N.; Wendoloski, J.J. A knowledge-based approach in designing combinatorial or medicinal chemistry libraries for drug discovery. 1. A qualitative and quantitative characterization of known drug databases. *J. Comb. Chem.* **1999**, *1*, 55–68. [\[CrossRef\]](#) [\[PubMed\]](#)
48. Veber, D.F.; Johnson, S.R.; Cheng, H.-Y.; Smith, B.R.; Ward, K.W.; Kopple, K.D. Molecular properties that influence the oral bioavailability of drug candidates. *J. Med. Chem.* **2002**, *45*, 2615–2623. [\[CrossRef\]](#) [\[PubMed\]](#)

49. Lampi, G.; Deidda, D.; Pinza, M.; Pompei, R. Enhancement of anti-herpetic activity of glycyrrhizic acid by physiological proteins. *Antivir. Chem. Chemother.* **2001**, *12*, 125–131. [[CrossRef](#)] [[PubMed](#)]
50. Lin, J.C. Mechanism of action of glycyrrhizic acid in inhibition of Epstein-Barr virus replication in vitro. *Antivir. Res.* **2003**, *59*, 41–47. [[CrossRef](#)]
51. Crance, J.M.; Scaramozzino, N.; Jouan, A.; Garin, D. Interferon, ribavirin, 6-azauridine and glycyrrhizin: Antiviral compounds active against pathogenic flaviviruses. *Antivir. Res.* **2003**, *58*, 73–79. [[CrossRef](#)]
52. Sasaki, H.; Takei, M.; Kobayashi, M.; Pollard, R.B.; Suzuki, F. Effect of glycyrrhizin, an active component of licorice roots, on HIV replication in cultures of peripheral blood mononuclear cells from HIV-seropositive patients. *Pathobiology* **2002**, *70*, 229–236. [[CrossRef](#)]
53. Miyake, K.; Tango, T.; Ota, Y.; Mitamura, K.; Yoshiba, M.; Kako, M.; Hayashi, S.; Ikeda, Y.; Hayashida, N.; Iwabuchi, S.; et al. Efficacy of Stronger Neo-Minophagen C compared between two doses administered three times a week on patients with chronic viral hepatitis. *J. Gastroenterol. Hepatol.* **2002**, *17*, 1198–1204. [[CrossRef](#)] [[PubMed](#)]
54. Yanagawa, Y.; Ogura, M.; Fujimoto, E.; Shono, S.; Okuda, E. Effects and cost of glycyrrhizin in the treatment of upper respiratory tract infections in members of the Japanese maritime self-defense force: Preliminary report of a prospective, randomized, double-blind, controlled, parallel-group, alternate-day treatment assignment clinical trial. *Curr. Res. Clin. Exp.* **2004**, *65*, 26–33. [[CrossRef](#)]
55. Chen, F.; Chan, K.H.; Jiang, Y.; Kao, R.Y.T.; Lu, H.T.; Fan, K.W.; Cheng, V.C.C.; Tsui, W.H.W.; Hung, I.F.N.; Lee, T.S.W. In vitro susceptibility of 10 clinical isolates of SARS coronavirus to selected antiviral compounds. *J. Clin. Virol.* **2004**, *31*, 69–75. [[CrossRef](#)] [[PubMed](#)]
56. Hoever, G.; Baltina, L.; Michaelis, M.; Kondratenko, R.; Baltina, L.; Tolstikov, G.A.; Doerr, H.W.; Cinatl, J. Antiviral activity of glycyrrhizic acid derivatives against SARS–coronavirus. *J. Med. Chem.* **2005**, *48*, 1256–1259. [[CrossRef](#)] [[PubMed](#)]
57. Russo, M.; Moccia, S.; Spagnuolo, C.; Tedesco, I.; Russo, G.L. Roles of flavonoids against coronavirus infection. *Chem. Interact.* **2020**, *328*, 109211. [[CrossRef](#)]
58. Kandeil, A.; Mostafa, A.; Kutkat, O.; Moatasim, Y.; Al-Karmalawy, A.A.; Rashad, A.A.; Kayed, A.E.; Kayed, A.E.; El-Shesheny, R.; Kayali, G.; et al. Bioactive Polyphenolic Compounds Showing Strong Antiviral Activities against Severe Acute Respiratory Syndrome Coronavirus 2. *Pathogens* **2021**, *10*, 758. [[CrossRef](#)]
59. Wu, C.; Liu, Y.; Yang, Y.; Zhang, P.; Zhong, W.; Wang, Y.; Wang, Q.; Xu, Y.; Li, M.; Li, X. Analysis of therapeutic targets for SARS-CoV-2 and discovery of potential drugs by computational methods. *Acta Pharm. Sin. B* **2020**, *10*, 766–788. [[CrossRef](#)] [[PubMed](#)]
60. Zhang, L.; Lin, D.; Sun, X.; Curth, U.; Drosten, C.; Sauerhering, L.; Becker, S.; Rox, K.; Hilgenfeld, R. Crystal structure of SARS-CoV-2 main protease provides a basis for design of improved alpha-ketoamide inhibitors. *Science* **2020**, *368*, 409–412. [[CrossRef](#)]
61. Suarez, D.; Diaz, N. SARS-CoV-2 Main Protease: A Molecular Dynamics Study. *J. Chem. Inf. Model.* **2020**, *60*, 5815–5831. [[CrossRef](#)]
62. Das, S.; Sarmah, S.; Lyndem, S.; Singha Roy, A. An investigation into the identification of potential inhibitors of SARS-CoV-2 main protease using molecular docking study. *J. Biomol. Struct. Dyn.* **2020**, *39*, 3347–3357. [[CrossRef](#)]
63. Srivastava, V.; Yadav, A.; Sarkar, P. Molecular docking and ADMET study of bioactive compounds of *Glycyrrhiza glabra* against main protease of SARS-CoV2. *Mater. Today: Proc.* **2020**. [[CrossRef](#)] [[PubMed](#)]
64. Chandel, V.; Raj, S.; Rathi, B.; Kumar, D. In Silico Identification of Potent COVID-19 Main Protease Inhibitors from FDA Approved Antiviral Compounds and Active Phytochemicals through Molecular Docking: A Drug Repurposing Approach. *Chem. Biol. Lett.* **2020**. [[CrossRef](#)]
65. Singh, A.; Mishra, A. Leucofedin a potential inhibitor against SARS CoV-2 Mpro. *J. Biomol. Struct. Dyn.* **2020**, *39*, 4427–4432. [[CrossRef](#)] [[PubMed](#)]
66. Mittal, L.; Kumari, A.; Srivastava, M.; Singh, M.; Asthana, S. Identification of potential molecules against COVID-19 main protease through structure-guided virtual screening approach. *J. Biomol. Struct. Dyn.* **2020**, *39*, 3662–3680. [[CrossRef](#)] [[PubMed](#)]
67. Rizzuti, B.; Grande, F.; Conforti, F.; Jimenez-Alesanco, A.; Ceballos-Laita, L.; Ortega-Alarcon, D.; Vega, S.; Reyburn, H.T.; Abian, O.; Velazquez-Campoy, A. Rutin Is a Low Micromolar Inhibitor of SARS-CoV-2 Main Protease 3CLpro: Implications for Drug Design of Quercetin Analogs. *Biomedicines* **2021**, *9*, 375. [[CrossRef](#)]
68. Ngo, S.T.; Quynh Anh Pham, N.; Thi Le, L.; Pham, D.-H.; Vu, V.V. Computational determination of potential inhibitors of SARS-CoV-2 main protease. *J. Chem. Inf. Modeling* **2020**. [[CrossRef](#)]
69. Ghosh, R.; Chakraborty, A.; Biswas, A.; Chowdhuri, S. Evaluation of green tea polyphenols as novel corona virus (SARS CoV-2) main protease (Mpro) inhibitors—an in silico docking and molecular dynamics simulation study. *J. Biomol. Struct. Dyn.* **2020**. [[CrossRef](#)]
70. Van de Sand, L.; Bormann, M.; Alt, M.; Schipper, L.; Heilingloh, C.S.; Steinmann, E.; Todt, D.; Dittmer, U.; Elsner, C.; Witzke, O. Glycyrrhizin Effectively Inhibits SARS-CoV-2 Replication by Inhibiting the Viral Main Protease. *Viruses* **2021**, *13*, 609. [[CrossRef](#)]
71. Yuce, M.; Cicek, E.; Inan, T.; Dag, A.B.; Kurkuoglu, O.; Sungur, F.A. Repurposing of FDA-approved drugs against active site and potential allosteric drug-binding sites of COVID-19 main protease. *Proteins: Struct. Funct. Bioinform.* **2021**. [[CrossRef](#)] [[PubMed](#)]
72. Zhao, Y.; Du, X.; Duan, Y.; Pan, X.; Sun, Y.; You, T.; Han, L.; Jin, Z.; Shang, W.; Yu, J.; et al. High-throughput screening identifies established drugs as SARS-CoV-2 PLpro inhibitors. *Protein Cell* **2021**. [[CrossRef](#)] [[PubMed](#)]
73. Parmar, P.; Rao, P.; Sharma, A.; Shukla, A.; Rawal, R.M.; Saraf, M.; Patel, B.V.; Goswami, D. Meticulous assessment of natural compounds from NPASS database for identifying analogue of GRL0617, the only known inhibitor for SARS-CoV2 papain-like protease (PLpro) using rigorous computational workflow. *Mol. Divers.* **2021**. [[CrossRef](#)]

74. Li, D.; Luan, J.; Zhang, L. Molecular docking of potential SARS-CoV-2 papain-like protease inhibitors. *Biochem. Biophys. Res. Commun.* **2021**, *538*, 72–79. [[CrossRef](#)]
75. Mitra, D.; Verma, D.; Mahakur, B.; Kamboj, A.; Srivastava, R.; Gupta, S.; Pandey, A.; Arora, B.; Pant, K.; Panneerselvam, P.; et al. Molecular docking and simulation studies of natural compounds of *Vitex negundo* L. against papain-like protease (PLpro) of SARS CoV-2 (coronavirus) to conquer the pandemic situation in the world. *J. Biomol. Struct. Dyn.* **2021**. [[CrossRef](#)] [[PubMed](#)]
76. Jamalan, M.; Barzegari, E.; Gholami-Borujeni, F. Structure-Based Screening to Discover New Inhibitors for Papain-like Proteinase of SARS-CoV-2: An In Silico Study. *J. Proteome Res.* **2021**, *20*, 1015–1026. [[CrossRef](#)] [[PubMed](#)]
77. Delre, P.; Caporuscio, F.; Saviano, M.; Mangiatordi, G.F. Repurposing Known Drugs as Covalent and Non-covalent Inhibitors of the SARS-CoV-2 Papain-Like Protease. *Front. Chem.* **2020**, *8*, 594009. [[CrossRef](#)] [[PubMed](#)]
78. Kumar, Y.; Singh, H. In silico identification and docking-based drug repurposing against the main protease of SARS-CoV-2, causative agent of COVID-19. *Biol. Med. Chem.* **2020**, *13*, 1210–1223. [[CrossRef](#)]
79. Surti, M.; Patel, M.; Adnan, M.; Moin, A.; Ashraf, S.A.; Siddiqui, A.J.; Snoussi, M.; Deshpande, S.; Reddy, M.N. Ilimaquinone (marine sponge metabolite) as a novel inhibitor of SARS-CoV-2 key target proteins in comparison with suggested COVID-19 drugs: Designing, docking and molecular dynamics simulation study. *RSC Adv.* **2020**, *10*, 37707–37720. [[CrossRef](#)]
80. Laskar, M.A.; Choudhury, M.D. Search for therapeutics against COVID 19 targeting SARS-CoV-2 papain-like protease: An in silico study. *Res. Square* **2020**, Preprint. [[CrossRef](#)]
81. Moghaddam, E.; Teoh, B.-T.; Sam, S.-S.; Lani, R.; Hassandarvish, P.; Chik, Z.; Yueh, A.; Abubakar, S.; Zandi, K. Baicalin, a metabolite of baicalein with antiviral activity against dengue virus. *Sci. Rep.* **2014**, *4*, 5452. [[CrossRef](#)] [[PubMed](#)]
82. Nayak, M.K.; Agrawal, A.S.; Bose, S.; Naskar, S.; Bhowmick, R.; Chakrabarti, S.; Sarkar, S.; Chawla-Sarkar, M. Antiviral activity of baicalin against influenza virus H1N1-pdm09 is due to modulation of NS1-mediated cellular innate immune responses. *J. Antimicrob. Chemother.* **2014**, *69*, 1298–1310. [[CrossRef](#)] [[PubMed](#)]
83. Oo, A.; Teoh, B.T.; Sam, S.S.; Bakar, S.A.; Zandi, K. Baicalein and baicalin as Zika virus inhibitors. *Arch. Virol.* **2019**, *164*, 585–593. [[CrossRef](#)]
84. Oo, A.; Rausalu, K.; Merits, A.; Higgs, S.; Vanlandingham, D.; Bakar, S.A.; Zandi, K. Deciphering the potential of baicalin as an antiviral agent for Chikungunya virus infection. *Antivir. Res.* **2018**, *150*, 101–111. [[CrossRef](#)]
85. Kitamura, K.; Honda, M.; Yoshizaki, H.; Yamamoto, S.; Nakane, H.; Fukushima, M.; Ono, K.; Tokunaga, T. Baicalin, an inhibitor of HIV-1 production in vitro. *Antivir. Res.* **1998**, *37*, 131–140. [[CrossRef](#)]
86. Elfiky, A.A. Ribavirin, Remdesivir, Sofosbuvir, Galidesivir, and Tenofovir against SARS-CoV-2 RNA dependent RNA polymerase (RdRp): A molecular docking study. *Life Sci.* **2020**, *253*, 117592. [[CrossRef](#)]
87. Rameshkumar, M.R.; Indu, P.; Arunagirinathan, N.; Venkatadri, B.; El-Serehy, H.A.; Ahmad, A. Computational selection of flavonoid compounds as inhibitors against SARS-CoV-2 main protease, RNA-dependent RNA polymerase and spike proteins: A molecular docking study. *Saudi J. Biol. Sci.* **2021**, *28*, 448–458. [[CrossRef](#)]
88. Singh, S.; Sk, M.F.; Sonawane, A.; Kar, P.; Sadhukhan, S. Plant-derived natural polyphenols as potential antiviral drugs against SARS-CoV-2 via RNA-dependent RNA polymerase (RdRp) inhibition: An in-silico analysis. *J. Biomol. Struct. Dyn.* **2020**. [[CrossRef](#)]
89. Mishra, A.; Rathore, A.S. RNA dependent RNA polymerase (RdRp) as a drug target for SARS-CoV2. *J. Biomol. Struct. Dyn.* **2021**. [[CrossRef](#)]
90. Arba, M.; Wahyudi, S.T.; Brunt, D.J.; Paradis, N.; Wu, C. Mechanistic insight on the remdesivir binding to RNA-Dependent RNA polymerase (RdRp) of SARS-cov-2. *Comput. Biol. Med.* **2021**, *129*, 104156. [[CrossRef](#)] [[PubMed](#)]
91. Parvez, M.S.A.; Karim, M.A.; Hasan, M.; Jaman, J.; Karim, Z.; Tahsin, T.; Hasan, M.N.; Hosen, M.J. Prediction of potential inhibitors for RNA-dependent RNA polymerase of SARS-CoV-2 using comprehensive drug repurposing and molecular docking approach. *Int. J. Biol. Macromol.* **2020**, *163*, 1787–1797. [[CrossRef](#)] [[PubMed](#)]
92. Jain, A.S.; Sushma, P.; Dharmashekar, C.; Beelagi, M.S.; Prasad, S.K.; Shivamallu, C.; Prasad, A.; Syed, A.; Marraiki, N.; Prasad, K.S. In silico evaluation of flavonoids as effective antiviral agents on the spike glycoprotein of SARS-CoV-2. *Saudi J. Biol. Sci.* **2021**, *28*, 1040–1051. [[CrossRef](#)] [[PubMed](#)]
93. Yu, S.; Zhu, Y.; Xu, J.; Yao, G.; Zhang, P.; Wang, M.; Zhao, Y.; Lin, G.; Chen, H.; Chen, L.; et al. Glycyrrhizic acid exerts inhibitory activity against the spike protein of SARS-CoV-2. *Phytomedicine* **2021**, *85*, 153364. [[CrossRef](#)]
94. Leung, K.; Shum, M.H.; Leung, G.M.; Lam, T.T.; Wu, J.T. Early transmissibility assessment of the N501Y mutant strains of SARS-CoV-2 in the United Kingdom, October to November 2020. *Eurosurveillance* **2021**, *26*, 2002106. [[CrossRef](#)]
95. Galloway, S.E.; Paul, P.; MacCannell, D.R.; Johansson, M.A.; Brooks, J.T.; MacNeil, A.; Slayton, R.B.; Tong, S.; Silk, B.J.; Armstrong, G.L. Emergence of SARS-CoV-2 b. 1.1. 7 lineage—United States, December 29, 2020–January 12, 2021. *Morb. Mortal. Wkly. Rep.* **2021**, *70*, 95. [[CrossRef](#)]
96. Paiva, M.H.S.; Guedes, D.R.D.; Docena, C.; Bezerra, M.F.; Dezordi, F.Z.; Machado, L.C.; Krokovsky, L.; Helvecio, E.; Da Silva, A.F.; Vasconcelos, L.R.S. Multiple Introductions Followed by Ongoing Community Spread of SARS-CoV-2 at One of the Largest Metropolitan Areas of Northeast Brazil. *Viruses* **2020**, *12*, 1414. [[CrossRef](#)] [[PubMed](#)]
97. Mwenda, M.; Saasa, N.; Sinyange, N.; Busby, G.; Chipimo, P.J.; Hendry, J.; Kapona, O.; Yingst, S.; Hines, J.Z.; Minchella, P.; et al. Detection of B.1.351 SARS-CoV-2 Variant Strain—Zambia, December 2020. *MMWR Morb. Mortal. Wkly. Rep.* **2021**, *70*, 280–282. [[CrossRef](#)] [[PubMed](#)]

98. Mujwar, S. Computational repurposing of tamibarotene against triple mutant variant of SARS-CoV-2. *Comput. Biol. Med.* **2021**, *136*, 104748. [[CrossRef](#)] [[PubMed](#)]
99. Mhatre, S.; Gurav, N.; Shah, M.; Patravale, V. Entry-inhibitory role of catechins against SARS-CoV-2 and its UK variant. *Comput. Biol. Med.* **2021**, *135*, 104560. [[CrossRef](#)] [[PubMed](#)]
100. Mirza, M.U.; Froeyen, M. Structural elucidation of SARS-CoV-2 vital proteins: Computational methods reveal potential drug candidates against main protease, Nsp12 polymerase and Nsp13 helicase. *J. Pharm. Anal.* **2020**, *10*, 320–328. [[CrossRef](#)]
101. Jia, Z.; Yan, L.; Ren, Z.; Wu, L.; Wang, J.; Guo, J.; Zheng, L.; Ming, Z.; Zhang, L.; Lou, Z. Delicate structural coordination of the Severe Acute Respiratory Syndrome coronavirus Nsp13 upon ATP hydrolysis. *Nucleic Acids Res.* **2019**, *47*, 6538–6550. [[CrossRef](#)]
102. Rowaiye, A.; Onuh, O.; Asala, T.; Ogu, A.; Bur, D.; Nwankwo, E.; Orji, U.; Ibrahim, Z.; Hamza, J.; Ugorji, A. In silico identification of potential allosteric inhibitors of the SARS-CoV-2 Helicase. *ChemRxiv. Prepr.* **2020**. [[CrossRef](#)]
103. Vivek-Ananth, R.P.; Krishnaswamy, S.; Samal, A. Potential phytochemical inhibitors of SARS-CoV-2 helicase Nsp13: A molecular docking and dynamic simulation study. *Mol. Divers.* **2021**, 1–14. [[CrossRef](#)]
104. Wang, Y.; Fang, S.; Wu, Y.; Cheng, X.; Zhang, L.-k.; Shen, X.-r.; Li, S.-q.; Xu, J.-r.; Shang, W.-j.; Gao, Z.-b.; et al. Discovery of SARS-CoV-2-E channel inhibitors as antiviral candidates. *Acta Pharmacol. Sin.* **2021**. [[CrossRef](#)] [[PubMed](#)]
105. Hoffmann, M.; Kleine-Weber, H.; Schroeder, S.; Krüger, N.; Herrler, T.; Erichsen, S.; Schiergens, T.S.; Herrler, G.; Wu, N.-H.; Nitsche, A. SARS-CoV-2 cell entry depends on ACE2 and TMPRSS2 and is blocked by a clinically proven protease inhibitor. *Cell* **2020**, *181*, 271–280.e278. [[CrossRef](#)] [[PubMed](#)]
106. Krieger, E.; Vriend, G. YASARA View—Molecular graphics for all devices—From smartphones to workstations. *Bioinformatics* **2014**, *30*, 2981–2982. [[CrossRef](#)]
107. Bilal, S.; Hassan, M.M.; Ur Rehman, M.F.; Nasir, M.; Sami, A.J.; Hayat, A. An insect acetylcholinesterase biosensor utilizing WO₃/g-C₃N₄ nanocomposite modified pencil graphite electrode for phosmet detection in stored grains. *Food Chem.* **2021**, *346*, 128894. [[CrossRef](#)]
108. Laskowski, R.A.; Swindells, M.B. LigPlot+: Multiple Ligand-Protein Interaction Diagrams for Drug Discovery. *J. Chem Infor. Modeling.* **2011**, *51*, 2778–2786. [[CrossRef](#)]
109. Fernandez-Poza, S.; Padros, A.; Thompson, R.; Butler, L.; Islam, M.; Mosely, J.; Scrivens, J.H.; Rehman, M.F.; Akram, M.S. Tailor-made recombinant prokaryotic lectins for characterisation of glycoproteins. *Anal. Chim. Acta* **2021**, *1155*, 338352. [[CrossRef](#)]
110. Motulsky, H. *Prism 4 Statistics Guide—Statistical Analyses for Laboratory and Clinical Researchers*; GraphPad Softw. Inc.: San Diego, CA, USA, 2003; pp. 122–126.